NACA

AUG 15 1947

RESEARCH MEMORANDUM

for the

Bureau of Aeronautics, Navy Department

INVESTIGATION OF SEA-LEVEL PERFORMANCE OF I-16 TURBOJET

ENGINE AT ZERO RAM WITH XFR-1 INTAKE DUCT

SHROUD, AND TAIL PIPE

By Harry W. Dowman and William G. Anderson

Flight Propulsion Research Laboratory
Cleveland, Ohio

NATIONAL ADVISORY COMMITTEE FOR AERONAUTICS

WASHINGTON

AUGUST 5 1947

NATIONAL ADVISORY COMMITTEE FOR AERONAUTICS

RESEARCH MEMORANDUM

for the

Bureau of Aeronautics, Navy Department

INVESTIGATION OF SEA-LEVEL PERFORMANCE OF I-16 TURBOJET

ENGINE AT ZERO RAM WITH XFR-1 INTAKE DUCT

SHROUD, AND TAIL PIPE

By Harry W. Dowman and William G. Anderson

SUMMARY

The sea-level performance of an I-16 turbojet engine at zero
ram was investigated to determine the effects of an intake duct, a
shroud, and a tail pipe intended for installation in an XFR-1 air-
plane. The investigation was conducted over a range of engine speeds
from 8000 to 16,500 rpm for several arrangements of the intake duct
and tail pipes: the XFR-1 duct, shroud, and tail pipe with the
boundary-layer slot closed and open and with boundary-layer removal
by suction; the XFR-1 duct with a tail pipe from a P-59A airplane
and boundary-layer removal; and with no intake duct or shroud with
both the P-59A and the XFR-1 tail pipes. The data were corrected to
standard atmospheric conditions and then adjusted to a common exhaust-
gas temperature.

The maximum total-pressure loss in the intake duct and shroud
of 3.36 percent of the ambient pressure, occurred with the boundary-
layer slot open at a corrected rotor speed of 16,500 rpm. The
attendant loss in thrust was 90 pounds. The intake-duct total-
pressure losses for the other three configurations with the duct
were between 2.64 and 2.70 percent of the ambient pressure with
accompanying thrust losses of 80 to 86 pounds at the same engine
rotor speed. The maximum thrust loss caused by the XFR-1 tail pipe,
as compared with the P-59A tail pipe, was 24 pounds at a corrected
rotor speed of 15,000 rpm. At maximum corrected rotor speed
(16,500 rpm) the thrust loss caused by the XFR-1 tail pipe was
13 pounds.

INTRODUCTION

At the request of the Bureau of Aeronautics, Navy Department, an investigation has been conducted to determine the effects of an intake duct, shroud, and tail pipe, intended for installation in the XFR-1 airplane, on the sea-level performance of an I-16 turbojet engine at zero ram over a range of engine speeds from 8000 to 16,500 rpm.

The performance of the engine fitted with the XFR-1 intake duct was investigated with the following arrangements of the boundary-layer-removal slot: (1) closed, (2) open to ambient-air conditions in the cell, and (3) open with the boundary layer removed by an exhauster. The results with these configurations are compared with the performance of the engine without an intake duct. The engine performance with the XFR-1 tail pipe and with a tail pipe from the P-59A airplane is also compared. Engine performance characteristics are adjusted to common exhaust-gas temperatures(after correction to standard inlet conditions) to provide an accurate basis of comparison.

INTAKE DUCT AND TAIL PIPES

A sketch of the XFR-1 intake duct and shroud is presented in figure 1. The general design of the duct was determined by the intended installation of an I-16 turbojet engine in the rear of the fuselage of the XFR-1 airplane. A duct inlet is provided for installation at the leading edge of each wing to admit air to the engine. The sharp bends necessitated by the widely separated inlets are provided with turning vanes to reduce pressure losses. Smooth inlet contours, such as those in the wing, were provided during the investigation by suitable inlet nozzles (fig. 1).

The construction of the joint between the duct and the shroud was such that an annular passage about 3/8 inch wide on a 26-inch diameter was provided for removal of the boundary layer in flight. The boundary-layer slot is illustrated in figure 1 where detail A shows the boundary-layer slot closed and detail B shows the boundary-layer slot open. The general arrangement of the equipment used for boundary-layer removal is shown in figure 2. A Roots-type exhauster powered by a variable-speed electric motor was connected to an annular chamber (detail A, fig. 2) through which the boundary layer was removed. The mass flow of air removed from the intake duct by the exhauster was controlled by varying the speed of the electric motor.

The XFR-1 and P-59A tail pipes and nozzles used in this investigation are shown in figure 3. The XFR-1 tail pipe is about twice the length of the P-59A tail pipe. The respective nozzles differ slightly in contour but have the same throat diameter.

APPARATUS AND PROCEDURE

Installation. - The general arrangement of the equipment is illustrated in figure 4. A photograph of the setup is presented in figure 5. The details of the engine installation and the methods employed to measure the important performance characteristics, that is, thrust, air flow, fuel flow, and rotor speed, are described in reference 1.

Instrumentation. - The sections and the stations at which the setup was instrumented for temperature and pressure measurements are shown in figure 6.

The pressures measured and the location, type, and number of pressure-measuring instruments were as follows:

(1) Ambient pressure P_0, 1 open-end tube in quiescent zone of cell

(2) Total pressure at section A of duct P_A, 10 total-pressure tubes, 5 at each duct inlet

(3) Total pressure at section B of duct P_B, 38 total-pressure tubes (10 rakes)

(4) Total pressure at section C of shroud P_C, 6 total-pressure tubes in shroud rake

(5) Compressor-inlet total pressure P_1, 36 total-pressure tubes, 4 equally spaced groups of 3 around front inlet screen and 8 equally spaced groups of 3 around rear inlet screen

The temperatures measured and the location, type, and number of thermocouples were as follows:

(1) Ambient temperature T_0, 2 stagnation thermocouples, 1 at center of each duct inlet

(2) Compressor-inlet temperature T_1, 12 unshielded thermocouples, 4 equally spaced around front compressor inlet, 8 equally spaced around rear compressor inlet

(3) Exhaust-gas indicated temperature T_7, 6 NACA shielded thermocouples connected in parallel, for which positions are shown in figure 3

Pressures were measured on multitube manometer panels. Simultaneous readings were obtained by photographing the entire panel. Temperatures were indicated by self-balancing potentiometers. Iron-constantan thermocouples were used for air-temperature measurements and chromel-alumel thermocouples for combustion-gas-temperature measurements.

Procedure. - The engine performance was determined over a range of engine speeds from 8000 to 16,500 rpm for the following tail-pipe and intake-duct configurations:

Configuration	Intake	Tail pipe and nozzle
A	XFR-1 duct, boundary-layer slot closed	XFR-1
B	XFR-1 duct, boundary-layer slot open	XFR-1
C	XFR-1 duct, boundary-layer removal by suction	XFR-1
D	XFR-1 duct, boundary-layer removal by suction	P-59A
E	No intake duct nor shroud	P-59A
F	No intake duct nor shroud	XFR-1

Configurations A and B were investigated with the setup illustrated in figure 4. With configuration B, air flowed into the intake duct through the boundary-layer slot and therefore removal of the boundary layer was prevented. Approximately 2 percent of the mass air flow through the intake duct (computed from volumetric displacement of exhauster) was removed through the boundary-layer slot at all engine speeds with configurations C and D.

SYMBOLS

The following symbols are used in this report: (For symbols used in appendixes A to D, see appendix A)

F   thrust, (lb)

f   specific fuel consumption, (lb)/(hr)(lb thrust)

N   rotor speed, (rpm)

P   total pressure, (lb)/(sq in. absolute)

T   total (or indicated) temperature, (^{O}R)

W_a air flow, (lb)/(sec)

W_f fuel flow, (lb)/(hr)

δ   ratio of ambient-air pressure to NACA standard sea-level pres-
        sure (14.7 lb/sq in. absolute)

θ   ratio of ambient-air temperature to NACA standard sea-level
        temperature (519° R)

Subscripts:

0   ambient (cell)

1   compressor inlets

7   tail pipe

8   jet

A   intake duct, section A

B   intake duct, section B

C   shroud, section C

c   corrected to standard inlet conditions and adjusted to common
        exhaust-gas indicated temperature

t   calculated from inlet total-pressure losses (theoretical data)
        based on common exhaust-gas temperature

METHODS OF CALCULATION

Correction to standard sea-level conditions. - All the per-
formance data were corrected to standard atmospheric conditions

(14.7 lb/sq in. absolute and 519° R). For the engine equipped with
the XFR-1 intake duct and shroud, the ambient conditions were
measured at the duct inlets. For the engine without the duct and
the shroud, the ambient pressure was measured at the compressor
inlets. Measurement of the ambient temperature at the compressor
inlets, however, would not have penalized the engine for heating
the inlet air by heat transfer from the compressor casing. Moreover,
the ambient-air temperature had to be measured indirectly because of
large temperature variations within the cell. Therefore, on the
assumption that the temperature rise between the cell and the
compressor inlet is the same whether or not the duct and the shroud
are installed, the ambient-air temperature was taken as the measured
compressor-inlet temperature T_1 minus the temperature rise in the
intake duct that occurred when the duct was installed (fig. 7).

The following corrected performance variables are used:

F/δ corrected thrust, (lb)

$f/\sqrt{\theta}$ corrected specific fuel consumption, (lb)/(hr)(lb thrust)

$N/\sqrt{\theta}$ corrected rotor speed, (rpm)

P/δ corrected total pressure, (lb)/(sq in. absolute)

T/θ corrected indicated temperature, (°R)

$W_a\sqrt{\theta}/\delta$ corrected air flow, (lb)/(sec)

$W_f/\delta\sqrt{\theta}$ corrected fuel flow, (lb)/(hr)

Adjustment of data to common exhaust-gas temperature required
because of intake-duct pressure loss. - For an engine equipped with
a fixed-size exhaust nozzle and operating at a given rotor speed,
pressure loss in the intake duct and tail pipe causes an increase
in exhaust-gas temperature. On the other hand, for an engine
operating at a given rotor speed, an increase in exhaust-nozzle size
causes a reduction in exhaust-gas temperature. Because the exhaust-
gas temperature is a limiting factor in engine operation, an engine
operating with intake-duct and tail-pipe pressure losses required
an increased exhaust-nozzle size to prevent exceeding the maximum
allowable exhaust-gas temperature at rated rotor speed.

It is therefore important when the results of this investiga-
tion are compared that they all be based on common exhaust-gas
temperatures. The common exhaust-gas temperatures selected for this
investigation were taken with configuration E (no intake duct nor

shroud, P-59A tail pipe). Adjustment of the performance data to
these temperatures consists in finding the increased nozzle sizes
required to obtain the desired common temperatures and then evaluating
the changes in performance variables resulting from these changes in
nozzle size.

Curves of performance variables against exhaust-nozzle diameter
for various intake-duct losses, tail-pipe losses, and rotor speeds
should be used to adjust the data to common exhaust-gas temperatures.
Because such curves were unavailable and their determination was
beyond the scope of the investigation, curves of performance variables
against exhaust-nozzle diameter plotted from the data of reference 1
were used. Use of the curves obtained from reference 1 imposes the
assumption that curves of performance with various intake-duct and
tail-pipe pressures losses are parallel to curves of performance with
no pressure loss.

Curves of exhaust-gas temperature against exhaust-nozzle diameter
for various rotor speeds (from reference 1) would provide a simple
basis for evaluating the necessary changes in exhaust-nozzle diameter.
This method proved to be somewhat inaccurate, however, and better
correlation of the data was obtained by calculating, from
equation (62) in appendix D, the exhaust-nozzle diameters required
to maintain common exhaust-gas temperatures for all test configura-
tions. The performance variables were adjusted by means of the
curves of performance variables against exhaust-nozzle diameter
(reference 1) once the adjusted exhaust-nozzle diameter was calculated.

Calculation of thrust from intake-duct pressure loss and basic
engine performance. - The analysis in appendix C develops an equa-
tion to evaluate the adjusted thrust from intake-duct pressure loss
and basic engine performance. Values of thrust calculated by means
of equation (51) (appendix C) checked very closely the adjusted
thrust determined by the method of data adjustment previously
described. Because of the close agreement of adjusted experimental
thrust and calculated thrust as shown in table I for configurations
A and B, calculated values of thrust for configurations C and D
(in which interference imposed by the boundary-layer-removal equip-
ment caused inaccurate thrust measurements) were considered reliable
for these configurations and are also included in table I.

Adjustment of data to common exhaust-gas temperature required
because of tail-pipe pressure loss. - Inasmuch as tail-pipe-pressure-
loss data were inadequate, no analysis was developed to assist in
adjustment of the data required because of exhaust-gas-temperature
differences caused by tail-pipe losses. Hence, adjustment of the
data was based on the curve of exhaust-gas temperature against

exhaust-nozzle diameter (reference 1). Negligible error results
from this procedure because of the relatively small temperature
differences resulting from tail-pipe losses.

RESULTS AND DISCUSSION

Intake-Duct Pressure Loss

Losses in total pressure from the intake-duct inlet to each of
the instrumented sections of the duct (section B, section C, and
station 1, fig. 6) are shown as percentage of ambient pressure in
figure 8. Comparison of figures 8(a) and 8(b) indicates that opening
the boundary-layer slot slightly reduces the total-pressure loss to
section B but appreciably increases the losses to section C and
station 1 (compressor inlets). These effects were probably caused
by flow of air into the duct through the boundary slot. Comparison
of figures 8(c) and 8(d) with 8(a) shows a slight increase in the
losses to section B, section C, and station 1 for the boundary-
layer-removal configurations C and D over those for the closed-
boundary-layer-slot configuration A. Boundary-layer removal up to
2 percent of the air flow was ineffective in reducing the duct pres-
sure loss.

Engine Performance

Performance data corrected to standard inlet conditions but
unadjusted to common exhaust-gas temperatures are presented in
figures 9 to 12, in which thrust, fuel flow, air flow, and exhaust-
gas indicated temperature are shown as functions of corrected rotor
speed. Data for configurations A, B, and F (fig. 9), configura-
tions C and F (fig. 10), and configurations D and E (fig. 11),
are compared. Because of the previously mentioned interference with
thrust measurement imposed by the equipment used to remove the
boundary layer, the thrust data for configurations C and D were
inaccurate; hence, thrust curves for these configurations have been
omitted. The thrust data from configurations E and F are
presented in figure 12. The performance curves as shown provide a
poor comparison of the configurations used because of variations in
exhaust-gas temperatures (figs. 9(d), 10(c), and 11(c)).

The exhaust-gas temperatures of configuration E (fig. 11(c)),
to which all the performance data are adjusted, are replotted in
figure 13 with an expanded speed scale.

CONFIDENTIAL

The adjusted, corrected performance data are presented in figures 14 to 16. Thrust curves calculated by the method described previously are shown in figures 15(a) and 16(a) for configurations C and D, respectively. Specific-fuel-consumption data (figs. 15(d) and 16(d)) were determined using these calculated values of thrust (figs. 15(a) and 16(a)).

The effect of the XFR-1 intake duct and shroud on the engine performance may be observed by comparing the performance variables of configurations A and B with those of configuration F in figure 14, the variables of configuration C with those of configuration F in figure 15, and the variables of configuration D with those of configuration E in figure 16. In general, because of attendant pressure loss, the effect of the intake duct is to decrease the static thrust, the fuel flow, and the air flow and to increase the specific fuel consumption.

As shown in the figures and summarized in table II, the losses in thrust with the four duct configurations were all about the same (from 80 to 90 lb at 16,500 rpm) and varied in a manner consistent with the variation in intake-duct total-pressure loss (2.64 to 3.36 percent of the duct-inlet pressure P_0). The largest loss in thrust occurred with the open-boundary-layer-slot configuration B. The losses in thrust (calculated) that occurred with boundary-layer-removal configurations C and D were 86 and 85 pounds for intake-duct total pressure losses of 2.70 and 2.65 percent of the duct-inlet pressure, respectively.

Thrust losses caused by the XFR-1 tail pipe as compared to the P-59A tail pipe may be observed by comparing the thrust for configuration E (P-59A tail pipe, fig. 16(a)) with the thrust for configuration F (XFR-1 tail pipe, fig. 14(a) or 15(a)) and are summarized in table III. The engine thrust was slightly greater with the P-59A tail pipe than with the XFR-1 tail pipe over the full range of rotor speeds with a maximum difference of 24 pounds at a rotor speed of 15,000 rpm and a difference of 13 pounds at maximum rotor speed (16,500 rpm).

SUMMARY OF RESULTS

An investigation of the performance of an I-16 turbojet engine equipped with the XFR-1 intake duct, shroud, and tail pipe showed the following results:

1. The maximum total-pressure loss in the intake duct and shroud of 3.36 percent of the ambient cell pressure occurred with the

boundary-layer slot open at a rotor speed of 16,500 rpm. The
attendant loss in thrust was 90 pounds. The intake-duct total-
pressure losses for the other three duct configurations were between
2.64 and 2.70 percent of the ambient cell pressure with accompanying
thrust losses of 80 to 86 pounds at the same engine rotor speed.

2. The maximum thrust loss caused by the XFR-1 tail pipe as
compared to the P-59A tail pipe, was 24 pounds at an engine rotor
speed of 15,000 rpm. The thrust loss at maximum engine rotor speed
(16,500 rpm) caused by the XFR-1 tail pipe was 13 pounds.

Flight Propulsion Research Laboratory,
        National Advisory Committee for Aeronautics,
                Cleveland, Ohio.

                                        Harry W. Dowman,
                                        Mechanical Engineer.

                                        William G. Anderson,
                                        Mechanical Engineer.

Approved:
                Eugene J. Manganiello,
                Mechanical Engineer.

                Benjamin Pinkel,
                        Physicist.
jh

APPENDIX A

SYMBOLS

In addition to the symbols defined in the text, the following symbols and necessary values are used in the analyses:

A   area, sq in.

C_a exhaust-nozzle-area coefficient

C_v exhaust-nozzle-velocity coefficient, ratio of actual jet velocity to ideal jet velocity

c_p specific heat of exhaust gas at constant pressure, Btu/(lb)($^\circ$F)

D   exhaust-nozzle diameter, in.

f/a   fuel-air ratio

g   acceleration of gravity, 32.2 ft/sec^2

hp_c compressor horsepower

hp_t turbine horsepower

J   mechanical equivalent of heat, 778 ft-lb/Btu

p   static pressure, lb/sq in. absolute

R   gas constant, ft-lb/(lb)($^\circ$F)

t   static temperature, $^\circ$R

V   velocity, ft/sec

W_g gas flow, lb/sec

ΔP_b burner pressure drop, lb/sq in.

η_c compressor efficiency

η_t turbine efficiency

γ ratio of specific heats of exhaust gas

NACA RM No. E7G24

Subscripts:

2   compressor outlet

5   turbine inlet

The stations referred to by numerical subscripts are shown in figure 6.

APPENDIX B

FUNDAMENTAL ANALYSIS OF TEMPERATURE, PRESSURE, AND

VELOCITY RELATIONS

The relations between temperature, pressure, and velocity that are required to develop the analysis of appendixes C and D are established in appendix B. In appendix C, an equation for calculating the engine thrust from intake-duct pressure-loss data and basic engine-performance data is derived. This analysis is extended in appendix D to develop an equation for calculating the exhaust-nozzle size required to maintain constant exhaust-gas temperature for various intake-duct pressure losses at a given engine speed.

The performance of a turbojet engine is determined by rotor speed N, compressor-inlet total temperature T_1, and any other given condition. For a given rotor speed N, compressor-inlet temperature T_1, and exhaust-gas temperature T_7 (obtained by variation of exhaust-nozzle area), all pressure ratios across the various components and all velocities and temperatures in the system (from compressor inlet to exhaust-nozzle inlet) are maintained constant.

Proof of the preceding statement follows:

$$N = \text{constant} \tag{1}$$

If the exhaust nozzle is adjusted,

$$T_5 = \text{constant} \tag{2}$$

For a given V_0 and T_0

$$T_1 = \text{constant} \tag{3}$$

From equation (1)

$$hp_c/W_a = \text{constant} \tag{4}$$

From equation (4)

$$T_2 - T_1 = \text{constant} \tag{5}$$

From equations (5) and (3)

$$T_2 = \text{constant} \tag{6}$$

From equations (2) and (6), if a constant combustion efficiency is assumed,

$$f/a = \text{constant} \qquad (7)$$

Because turbine power is equal to compressor power, from equation (4)

$$hp_t/W_a = \text{constant} \qquad (8)$$

Now

$$T_5 - T_7 \propto \frac{hp_t/W_a}{1 + (f/a)} \qquad (9)$$

so from equations (7), (8), and (9)

$$T_5 - T_7 = \text{constant} \qquad (10)$$

From equations (2) and (10)

$$T_7 = \text{constant} \qquad (11)$$

If sonic flow through the turbine-nozzle throat is assumed,

$$W_a = \frac{1}{[1 + (f/a)]} \sqrt{2g \, \frac{\gamma}{\gamma + 1} \left(\frac{2}{\gamma + 1}\right)^{\frac{2}{\gamma - 1}} \frac{P_5 \, A_5}{\sqrt{RT_5}}} \qquad (12)$$

or

$$W_a \propto P_5 \qquad (13)$$

Now

$$P_5 = P_2 - \Delta P_b = P_2 \left(1 - \frac{\Delta P_b}{P_2}\right) \qquad (14)$$

However

$$\Delta P_b/P_2 = \phi_1(V_2, T_2, T_5) = \phi_2(V_2) \qquad (15)$$

From equations (13), (14), and (15)

$$W_a \propto P_2 \, \phi_3(V_2) \qquad (16)$$

From the equation of state at station 2 and the relation between static and total conditions,

$$W_a = \frac{P_2 A_2 V_2}{RT_2} \left(1 - \frac{V_2^2}{2gJc_pT_2}\right)^{\frac{1}{\gamma-1}}$$

$$= P_2 \, \phi_4(V_2) \tag{17}$$

Because, in general, ϕ_3 and ϕ_4 in equations (16) and (17) are not the same function

$$V_2 = \text{constant} \tag{18}$$

From equation (17)

$$W_a/P_2 = \text{constant} \tag{19}$$

From equation (15)

$$\Delta P_b/P_2 = \text{constant} \tag{20}$$

From the equation of state

$$W_a = \frac{P_1 V_1 A_1}{RT_1} \left(1 - \frac{V_1^2}{2gJc_pT_1}\right)^{\frac{1}{\gamma-1}}$$

or

$$W_a \propto P_1 \, \phi_5(V_1) \tag{21}$$

From equation (19)

$$W_a \propto P_2 \propto P_1 \frac{P_2}{P_1} \tag{22}$$

Now

$$P_2/P_1 = \phi_6\left(\frac{hp_c}{W_a}, T_1, \eta_c\right) \tag{23}$$

and

$$\eta_c = \phi_7(V_1, T_1, N) \tag{24}$$

If equations (23) and (24) are combined

$$P_2/P_1 = \phi_8(V_1) \tag{25}$$

and if equations (25) and (22) are combined

$$W_a \propto P_1 \phi_8(V_1) \tag{26}$$

Because, in general, ϕ_5 and ϕ_8 in equations (21) and (26), respectively, are not the same function

$$V_1 = \text{constant} \tag{27}$$

$$W_a/P_1 = \text{constant} \tag{28}$$

In a similar manner it can be shown that

$$V_5 = \text{constant} \tag{29}$$

$$\eta_t = \text{constant} \tag{30}$$

$$P_5/P_7 = \text{constant} \tag{31}$$

and also that

$$V_7 = \text{constant} \tag{32}$$

From these equations therefore

$$t_1, \ t_2, \ t_5, \ t_7, \ T_1, \ T_2, \ T_5, \ T_7 = \text{constants} \tag{33}$$

$$V_1, \ V_2, \ V_5, \ V_7 = \text{constants} \tag{34}$$

$$\frac{P_2}{P_1}, \ \frac{P_5}{P_2}, \ \frac{P_5}{P_7}, \ \frac{P_7}{P_1} = \text{constants} \tag{35}$$

APPENDIX C

DERIVATION OF EQUATION FOR CALCULATING ENGINE THRUST

FROM INTAKE-DUCT PRESSURE-LOSS DATA AND

BASIC ENGINE-PERFORMANCE DATA

An equation for calculating the engine thrust from intake-duct pressure-loss data and basic engine-performance data is derived in the following analysis. The subscript n in this appendix and appendix D refers to the condition in which there are no inlet losses. In general, symbols lacking this subscript apply to the condition in which inlet losses exist. Symbols of quantities that do not vary with intake-duct pressure losses also lack this subscript.

The actual jet velocity with no inlet losses is

$$V_{8,n} = C_v \sqrt{2gJc_pT_7 \left[1 - \left(\frac{p_8}{P_{7,n}}\right)^{\frac{\gamma-1}{\gamma}}\right]} \tag{37}$$

The jet velocity with inlet losses (using equation (11)) is

$$V_8 = C_v \sqrt{2gJc_pT_7 \left[1 - \left(\frac{p_8}{P_7}\right)^{\frac{\gamma-1}{\gamma}}\right]} \tag{38}$$

The net thrust without inlet losses is

$$F_n = \frac{W_{g,n}}{g} V_{8,n} - \frac{W_{a,n}}{g} V_0 \tag{39}$$

From equations (37) and (39)

$$\left(\frac{p_8}{P_{7,n}}\right)^{\frac{\gamma-1}{\gamma}} = \left[1 - \frac{\left(\frac{gF_n}{W_{g,n}} + \frac{W_{a,n}}{W_{g,n}} V_0\right)^2}{C_v^2 2gJc_pT_7}\right] \tag{40}$$

From equation (35)

$$\frac{P_{7,n}}{P_{1,n}} = \frac{P_7}{P_1} \tag{41}$$

and because

$$P_{1,n} = P_0$$

$$P_{7,n} = \frac{P_0}{P_1} \tag{42}$$

or

$$\frac{p_8}{P_{7,n}} = \frac{p_8}{P_7} \frac{P_1}{P_0} \tag{43}$$

When equation (43) is substitited in equation (40)

$$\left(\frac{p_8}{P_7}\right)^{\frac{\gamma-1}{\gamma}} = \left(\frac{P_0}{P_1}\right)^{\frac{\gamma-1}{\gamma}} \left[1 - \frac{\left(\frac{gF_n}{W_{g,n}} + \frac{W_{a,n}}{W_{g,n}} V_0\right)^2}{C_v^2 2gJc_pT_7}\right] \tag{44}$$

With inlet losses

$$F_t = \frac{W_g}{g} V_8 - \frac{W_a}{g} V_0 \tag{45}$$

From equations (38) and (45)

$$V_8 = \frac{gF_t}{W_g} + \frac{W_a}{W_g} V_0 = C_v \sqrt{2gJc_pT_7 \left[1 - \left(\frac{p_8}{P_7}\right)^{\frac{\gamma-1}{\gamma}}\right]} \tag{46}$$

From equations (44) and (46)

$$g\frac{F_t}{W_g} = C_v \sqrt{2gJc_pT_7 \left\{1 - \left[1 - \frac{\left(\frac{gF_n}{W_{g,n}} + \frac{W_a}{W_{g,n}} V_0\right)^2}{C_v^2 2gJc_pT_7}\right]\left(\frac{P_0}{P_1}\right)^{\frac{\gamma-1}{\gamma}}\right\}} - \frac{W_a}{W_g} V_0 \tag{47}$$

$$g\frac{F_t}{W_g} = \left(\frac{P_1}{P_0}\right)^{\frac{1-\gamma}{2\gamma}} \sqrt{\left[\left(\frac{P_1}{P_0}\right)^{\frac{\gamma-1}{\gamma}} - 1\right]C_v^2 2gJc_pT_7 + \left(\frac{gF_n}{W_{g,n}} + \frac{W_{a,n}}{W_{g,n}}V_0\right)^2} - \frac{W_a}{W_g}V_0 \quad (48)$$

Because, from equation (28),

$$\frac{W_g}{W_{g,n}} = \frac{P_1}{P_0} = \frac{W_a}{W_{a,n}} \quad (49)$$

then

$$F_t = \frac{W_{g,n}}{g}\left(\frac{P_1}{P_0}\right)^{\frac{1+\gamma}{2\gamma}} \sqrt{\left[\left(\frac{P_1}{P_0}\right)^{\frac{\gamma-1}{\gamma}} - 1\right]C_v^2 2gJc_pT_7 + \left(\frac{gF_n}{W_{g,n}} + \frac{W_{a,n}}{W_{g,n}}V_0\right)^2} - \frac{P_1}{P_0}\frac{W_{a,n}}{g}V_0 \quad (50)$$

If $P_1 = P_0 - (P_0 - P_1)$ is substituted for $V_0 = 0$ (zero ram)

$$F_t = \left(1 - \frac{P_0 - P_1}{P_0}\right)^{\frac{1+\gamma}{2\gamma}} \sqrt{\left(\frac{W_{g,n}}{g}\right)^2 C_v^2 2gJc_pT_7\left[\left(1 - \frac{P_0 - P_1}{P_0}\right)^{\frac{\gamma-1}{\gamma}} - 1\right] + F_n^2} \quad (51)$$

APPENDIX D

DERIVATION OF EQUATION FOR CALCULATING EXHAUST-NOZZLE SIZES

REQUIRED TO MAINTAIN CONSTANT EXHAUST-GAS TEMPERATURE

FOR VARIOUS INTAKE-DUCT PRESSURE LOSSES

An equation for calculating the exhaust-nozzle sizes required
to maintain constant exhaust-gas temperature for various intake-duct
pressure losses is developed.

From the equation of state at the exhaust-nozzle throat (jet)
for the engine operating with no inlet losses

$$C_{a,n} \, A_{8,n} = \frac{W_{g,n} \, R \, t_{8,n}}{p_8 \, V_{8,n}} \tag{52}$$

With inlet losses

$$C_a \, A_8 = \frac{W_g \, R \, t_8}{p_8 \, V_8} \tag{53}$$

If the exhaust-nozzle-area coefficient is assumed to remain the same
(that is, $C_{a,n} = C_a$), then

$$\frac{A_8}{A_{8,n}} = \frac{W_g \, t_8 \, V_{8,n}}{W_{g,n} \, t_{8,n} \, V_8} \tag{54}$$

Now (from equation (28))

$$\frac{W_g}{W_{g,n}} = \frac{P_1}{P_0} \tag{55}$$

And from the general energy equation and equations (33), (37),
and (38)

$$\frac{t_8}{t_{8,n}} = \frac{T_7 \left(1 - \dfrac{V_8^2}{2gJc_p T_7} \right)}{T_7 \left(1 - \dfrac{V_{8,n}^2}{2gJc_p T_7} \right)} = \frac{1 - C_v^2 \left[1 - \left(\dfrac{p_8}{p_7} \right)^{\frac{\gamma - 1}{\gamma}} \right]}{1 - C_v^2 \left[1 - \left(\dfrac{p_8}{p_{7,n}} \right)^{\frac{\gamma - 1}{\gamma}} \right]} \tag{56}$$

From equations (37) and (38)

$$\frac{V_{8,n}}{V_8} = \left[\frac{1 - \left(\frac{p_8}{P_{7,n}}\right)^{\frac{\gamma-1}{\gamma}}}{1 - \left(\frac{p_8}{P_7}\right)^{\frac{\gamma-1}{\gamma}}} \right]^{\frac{1}{2}} \tag{57}$$

Substituting equations (55), (56), and (57) in equation (54) gives

$$\frac{A_8}{A_{8,n}} = \left(\frac{P_1}{P_0}\right) \left\{ \frac{1 - C_v^2 \left[1 - \left(\frac{p_8}{P_7}\right)^{\frac{\gamma-1}{\gamma}} \right]}{1 - C_v^2 \left[1 - \left(\frac{p_8}{P_{7,n}}\right)^{\frac{\gamma-1}{\gamma}} \right]} \right\} \left[\frac{1 - \left(\frac{p_8}{P_{7,n}}\right)^{\frac{\gamma-1}{\gamma}}}{1 - \left(\frac{p_8}{P_7}\right)^{\frac{\gamma-1}{\gamma}}} \right]^{\frac{1}{2}} \tag{58}$$

From equations (40) and (44)

$$\frac{1 - \left(\frac{p_8}{P_{7,n}}\right)^{\frac{\gamma-1}{\gamma}}}{1 - \left(\frac{p_8}{P_7}\right)^{\frac{\gamma-1}{\gamma}}} = \frac{\dfrac{\left(\dfrac{gF_n}{W_{g,n}} + \dfrac{W_{a,n}}{W_{g,n}} V_0\right)^2}{C_v^2 2gJc_p T_7} \left(\dfrac{P_1}{P_0}\right)^{\frac{\gamma-1}{\gamma}}}{\left[\left(\dfrac{P_1}{P_0}\right)^{\frac{\gamma-1}{\gamma}} - 1 + \dfrac{\left(\dfrac{gF_n}{W_{g,n}} + \dfrac{W_{a,n}}{W_{g,n}} V_0\right)^2}{C_v^2 2gJc_p T_7} \right]} \tag{59}$$

Substituting equations (40), (44), and (59), in (58) gives

$$\frac{D^2}{D_n{}^2} = \frac{A_8}{A_{8,n}} = \left(\frac{P_1}{P_0}\right) \left[\frac{\left(\frac{P_1}{P_0}\right)^{\frac{\gamma-1}{\gamma}} \frac{\left(\frac{gF_n}{W_{g,n}} + \frac{W_{a,n}}{W_{g,n}} V_0\right)^2}{C_v{}^2 2gJc_pT_7}}{\left(\frac{P_1}{P_0}\right)^{\frac{\gamma-1}{\gamma}} - 1 + \frac{\left(\frac{gF_n}{W_{g,n}} + \frac{W_{a,n}}{W_{g,n}} V_0\right)^2}{C_v{}^2 2gJc_pT_7}}\right]^{\frac{1}{2}} \frac{1 - C_v{}^2 \left[1 - \frac{\left(\frac{gF_n}{W_{g,n}} + \frac{W_{a,n}}{W_{g,n}} V_0\right)^2}{\frac{C_v{}^2 2gJc_pT_7}{\left(\frac{P_1}{P_0}\right)^{\frac{\gamma-1}{\gamma}}}}\right]}{1 - C_v{}^2 \left[\frac{\left(\frac{gF_n}{W_{g,n}} + \frac{W_{a,n}}{W_{g,n}} V_0\right)^2}{C_v{}^2 2gJc_pT_7}\right]}$$

$$(60)$$

when $C_v{}^2$ in the numerator and the denominator of the last term of equation (60) is equal to unity, negligible error is introduced and equation (60) is simplified to

$$\frac{D^2}{D_n{}^2} = \left[\frac{\left(\frac{P_1}{P_0}\right)^{\frac{\gamma+1}{\gamma}} \frac{\left(\frac{gF_n}{W_{g,n}} + \frac{W_{a,n}}{W_{g,n}} V_0\right)^2}{C_v{}^2 2gJc_pT_7}}{\left(\frac{P_1}{P_0}\right)^{\frac{\gamma-1}{\gamma}} + \frac{\left(\frac{gF_n}{W_{g,n}} + \frac{W_{a,n}}{W_{g,n}} V_0\right)^2}{C_v{}^2 2gJc_pT_7} - 1}\right]^{\frac{1}{2}}$$

$$(61)$$

If P_1/P_0 is expressed as $1 - \dfrac{P_0 - P_1}{P_0}$ for the case of zero ram $V_0 = 0$

$$D = D_n \sqrt{\dfrac{\left(1 - \dfrac{P_0 - P_1}{P_0}\right)^{\frac{\gamma + 1}{2\gamma}} \dfrac{\left(\dfrac{gF_n}{W_{g,n}}\right)}{\sqrt{C_v{}^2 2gJc_pT_7}}}{\left[\dfrac{\left(\dfrac{gF_n}{W_{g,n}}\right)^2}{C_v{}^2 2gJc_pT_7} + \left(1 - \dfrac{P_0 - P_1}{P_0}\right)^{\frac{\gamma - 1}{\gamma}} - 1\right]^{\frac{1}{2}}}} \tag{62}$$

REFERENCE

1. Jones, William L., and Dowman, Harry W.: Experimental Investigation of a 1600-Pound Thrust Centrifugal-Flow-Type Turbojet Engine by Injection of Refrigerants at Compressor Inlets. NACA RM No. E7G23, 1947.

TABLE I – ADJUSTED EXPERIMENTAL THRUST AND THRUST CALCULATED FROM INTAKE-DUCT TOTAL-

PRESSURE LOSSES FOR I-16 ENGINE WITH XFR-1 INTAKE DUCT AND SHROUD

Corrected rotor speed $N/\sqrt{\theta}$ (rpm)	Exhaust-gas indicated temperature $T_{7,c}$ (°R)	Configuration A: Boundary-layer slot closed, XFR-1 tail pipe			Configuration B: Boundary-layer slot open, XFR-1 tail pipe			Configuration C: Boundary-layer removal, XFR-1 tail pipe [1]		Configuration D: Boundary-layer removal, P-59A tail pipe [1]	
		Duct total-pressure loss $\dfrac{P_0 - P_1}{P_0}$ (percent)	Calculated static thrust F_t (lb)	Adjusted static test thrust F_c (lb)	Duct total-pressure loss $\dfrac{P_0 - P_1}{P_0}$ (percent)	Calculated static thrust F_t (lb)	Adjusted static test thrust F_c (lb)	Duct total-pressure loss $\dfrac{P_0 - P_1}{P_0}$ (percent)	Calculated static thrust F_t (lb)	Duct total-pressure loss $\dfrac{P_0 - P_1}{P_0}$ (percent)	Calculated static thrust F_t (lb)
12,000	1398	1.12	533	533	1.36	527	530	1.10	533	1.10	541
13,000	1414	1.37	649	652	1.68	641	640	1.36	649	1.36	653
14,000	1445	1.66	794	798	2.04	791	793	1.66	794	1.65	806
15,000	1502	2.01	975	980	2.51	969	978	2.02	974	1.99	999
16,000	1584	2.42	1237	1243	3.07	1228	1230	2.44	1236	2.41	1246
16,500	1630	2.84	1382	1387	3.36	1372	1377	2.70	1381	2.65	1395

[1] Thrust measurements inaccurate because of interference of boundary-layer-removal equipment with thrust-measuring device.

NATIONAL ADVISORY
COMMITTEE FOR AERONAUTICS

TABLE II - THRUST LOSSES CAUSED BY INTAKE-DUCT TOTAL-PRESSURE LOSSES

Corrected rotor speed, $N/\sqrt[4]{\theta}$ (rpm)	Adjusted exhaust-gas indicated temperature $T_{7,c}$ ($^{\circ}$R)	Configuration A: Boundary-layer slot closed, XFR-1 tail pipe				Configuration B: Boundary-layer slot open, XFR-1 tail pipe			
		Adjusted static thrust, configuration A F_c (lb)	Adjusted static thrust, configuration F F_c (lb)	Thrust loss ΔF (lb)	Duct total-pressure loss $\dfrac{P_0 - P_1}{P_0}$ (percent)	Adjusted static thrust, configuration B F_c (lb)	Adjusted static thrust, configuration F F_c (lb)	Thrust loss ΔF (lb)	Duct total-pressure loss $\dfrac{P_0 - P_1}{P_0}$ (percent)
12,000	1398	533	558	25	1.12	530	558	28	1.36
13,000	1414	652	682	30	1.37	640	682	42	1.68
14,000	1445	798	837	39	1.66	793	837	44	2.04
15,000	1502	980	1030	50	2.01	978	1030	52	2.51
16,000	1584	1243	1310	67	2.42	1230	1310	80	3.07
16,500	1630	1387	1467	80	2.64	1377	1467	90	3.36

National Advisory Committee
for Aeronautics

TABLE II - THRUST LOSSES CAUSED BY INTAKE-DUCT TOTAL-PRESSURE LOSSES - Concluded

Corrected rotor speed, $N/\sqrt{\theta}$ (rpm)	Adjusted exhaust-gas indicated temperature $T_{7,c}$ ($^{\circ}R$)	Configuration C: Boundary-layer removal, XFR-1 tail pipe				Configuration D: Boundary-layer removal, P-59A tail pipe			
		Calculated static thrust, configuration C F_t (lb)	Adjusted static thrust, configuration F F_c (lb)	Thrust loss ΔF (lb)	Duct total-pressure loss $\dfrac{P_0 - P_1}{P_0}$ (percent)	Calculated thrust, configuration D F_t (lb)	Adjusted static thrust, configuration E F_c (lb)	Thrust loss ΔF (lb)	Duct total-pressure loss $\dfrac{P_0 - P_1}{P_0}$ (percent)
12,000	1398	533	558	25	1.10	541	566	25	1.10
13,000	1414	649	682	33	1.36	653	686	33	1.36
14,000	1445	794	837	43	1.66	806	848	42	1.65
15,000	1502	974	1030	56	2.02	999	1054	55	1.99
16,000	1584	1236	1310	74	2.44	1246	1319	73	2.41
16,500	1630	1381	1467	86	2.70	1395	1480	85	2.65

National Advisory Committee
for Aeronautics

TABLE III - THRUST LOSSES CAUSED BY XFR-1 TAIL

PIPE AS COMPARED WITH P-59A TAIL PIPE

Corrected rotor speed, $N/\sqrt{\theta}$ (rpm)	Adjusted exhaust-gas indicated temperature $T_{7,c}$ (^oR)	Adjusted static thrust, config-uration E, P-59A tail pipe F_c (1b)	Adjusted static thrust, config-uration F, XFR-1 tail pipe F_c (1b)	Thrust loss ΔF (1b)
12,000	1398	566	558	8
13,000	1414	686	682	4
14,000	1445	848	837	11
15,000	1502	1054	1030	24
16,000	1584	1319	1310	9
16,500	1630	1480	1467	13

National Advisory Committee
for Aeronautics

INDEX OF FIGURES

Figure 10. - Comparison of I-16 turbojet engine performance with removal of boundary layer from XFR-1 intake duct and with intake duct and shroud removed. XFR-1 tail pipe and nozzle.
(a) Fuel flow.
(b) Air flow.
(c) Exhaust-gas indicated temperature.

Figure 11. - Comparison of I-16 turbojet engine performance with removal of boundary layer from XFR-1 intake duct and with intake duct and shroud removed. P-59A tail pipe and nozzle.
(a) Fuel flow.
(b) Air flow.
(c) Exhaust-gas indicated temperature.

Figure 12. - Comparison of thrust of I-16 turbojet engine equipped with P-59A tail pipe and nozzle and with the XFR-1 tail pipe and nozzle. No intake duct nor shroud.

Figure 13. - Exhaust-gas indicated temperature for configuration E to which data from other configurations were adjusted. P-59A tail pipe and nozzle; no intake duct nor shroud. (Replotted from fig. 11(c).)

Figure 14. - Comparison of adjusted I-16 turbojet engine performance with XFR-1 intake duct in two positions and with intake duct and shroud removed. XFR-1 tail pipe and nozzle. Data adjusted to exhaust-gas indicated temperature of configuration E.
(a) Thrust.
(b) Fuel flow.
(c) Air flow.
(d) Specific fuel consumption.

Figure 15. - Comparison of adjusted I-16 turbojet engine performance with removal of boundary layer from XFR-1 intake duct and with intake duct and shroud removed. XFR-1 tail pipe and nozzle. Data adjusted to exhaust-gas indicated temperature of configuration E.
(a) Thrust.
(b) Fuel flow.
(c) Air flow.
(d) Specific fuel consumption.

Figure 16. - Comparison of adjusted I-16 turbojet engine performance with removal of boundary layer from XFR-1 intake duct and with intake duct and shroud removed. P-59A tail pipe and nozzle. Data adjusted to exhaust-gas indicated temperature of configuration E.
(a) Thrust.
(b) Fuel flow.
(c) Air flow.
(d) Specific fuel consumption.

NATIONAL ADVISORY
COMMITTEE FOR AERONAUTICS

Observation windows

Intake duct

Duct inlets

Inlet nozzles

$51\frac{1}{2}$"

$47\frac{1}{8}$"

$28\frac{1}{2}$"

135"

$54\frac{1}{2}$" $32\frac{1}{2}$"

$45\frac{1}{2}$" O. D.

Shroud

Turning vanes

(a) Top view.

8"R

Detail A
Boundary-layer-
removal slot closed

Detail B
Boundary-layer-
removal slot open

12"   30" $61\frac{3}{4}$" $39\frac{3}{4}$"

Boundary-layer-
removal slot
(See details A and B)

Duct
inlet

24"

4"

Inlet nozzle

$26\frac{1}{4}$" I.D.

$23\frac{1}{2}$" I.D.

Intake duct

(b) Side view.   25"

Shroud   Engine

Figure I. - XFR-I intake duct and shroud.

Fig. I

Fig. 2

Annulus around
boundary-layer-removal
slot

Shroud

Intake duct

Detail A

Detail A

Intake duct

Inlet nozzle

Variable-speed motor

Shroud

Roots-type exhauster

Figure 2. - General arrangement of equipment used for boundary-layer removal.
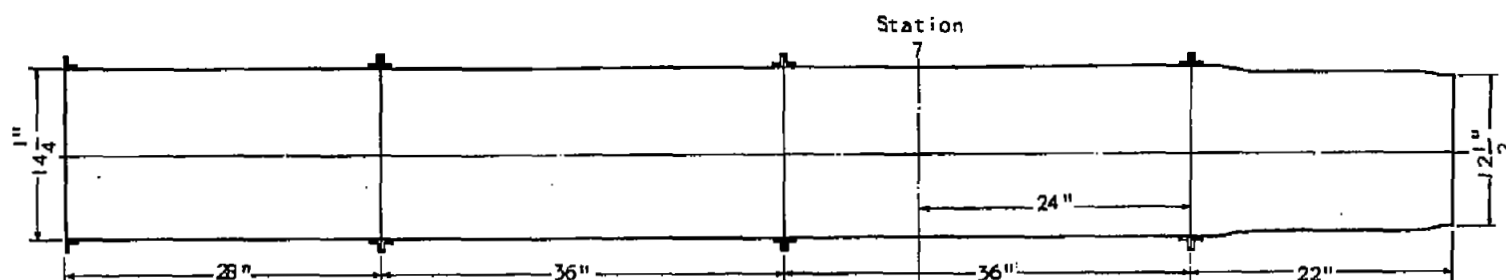
XFR-I tail pipe
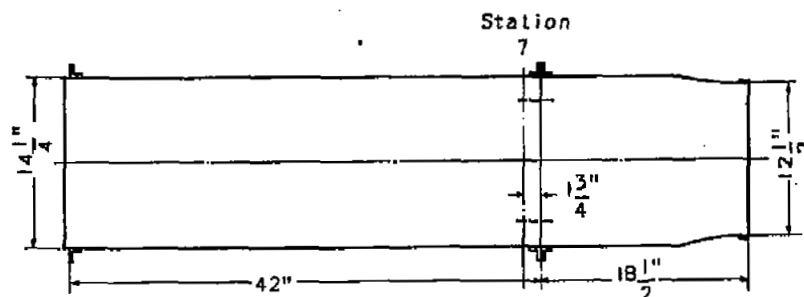
P-59A tail pipe

(a) Tail pipes.
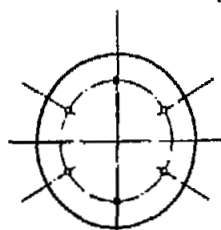
Station 7
XFR-I tail pipe
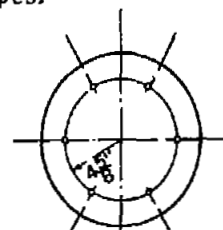
Station 7
P-59A tail pipe

(b) Arrangement of thermocouples at station 7; thermocouples connected in parallel.

Figure 3. - Configurations and instrumentation of XFR-I and P-59A tail pipes used in sea-level investigation at zero ram of I-16 turbojet engine with XFR-I intake duct and shroud.

Fig. 3
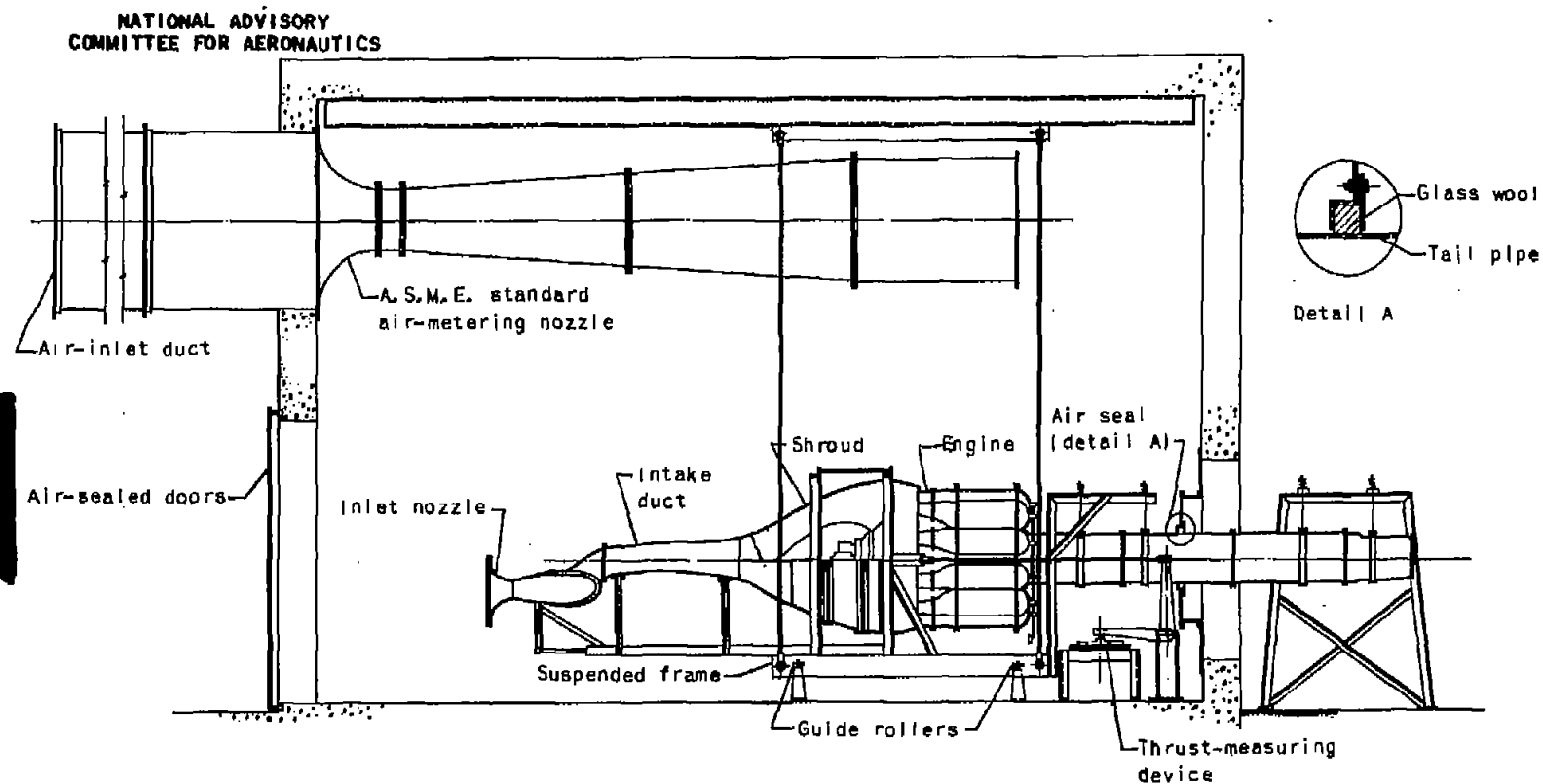
Figure 4. - General arrangement of equipment for sea-level investigation at zero ram of I-16 turbojet engine with XFR-1 intake duct, shroud, and tail pipe.

Fig. 4

801
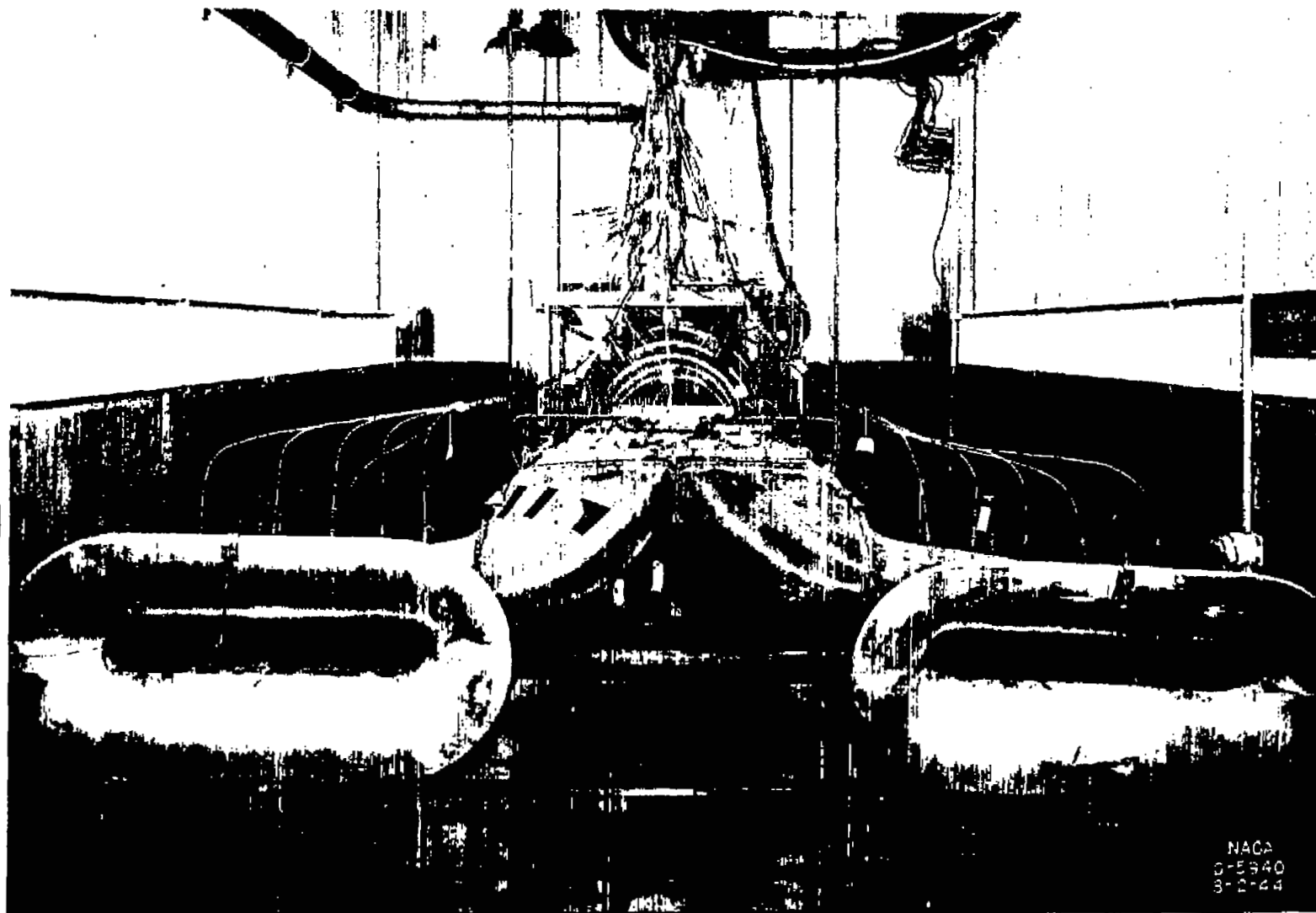
Figure 5. - Front view of setup for sea-level investigation at zero ram of I-16 turbojet engine with XFR-1 intake duct, shroud, and tail pipe.

Fig. 5
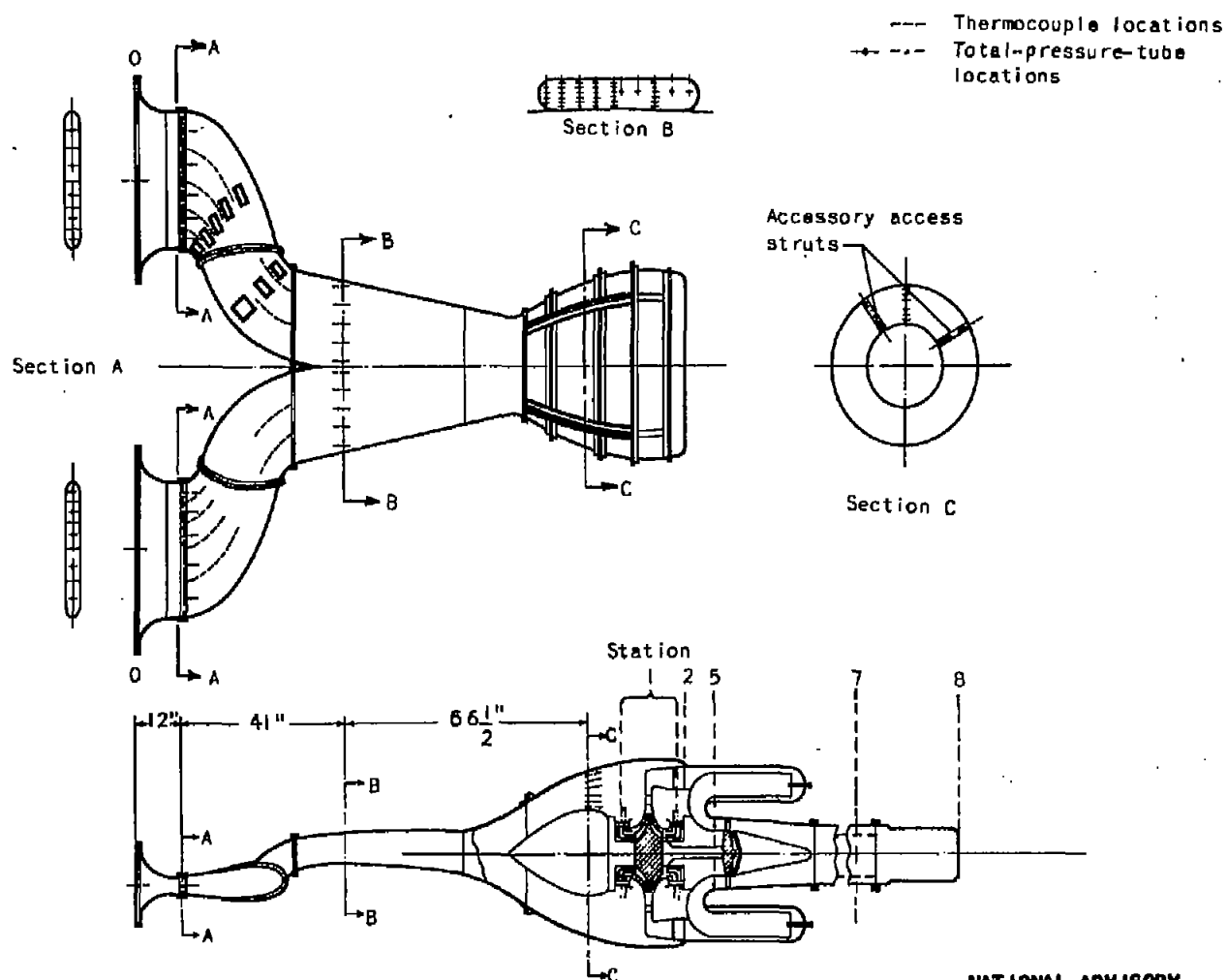
Figure 6. - Instrumentation of sections of XFR-1 intake duct and shroud and stations of I-16 turbojet engine.

Fig. 6
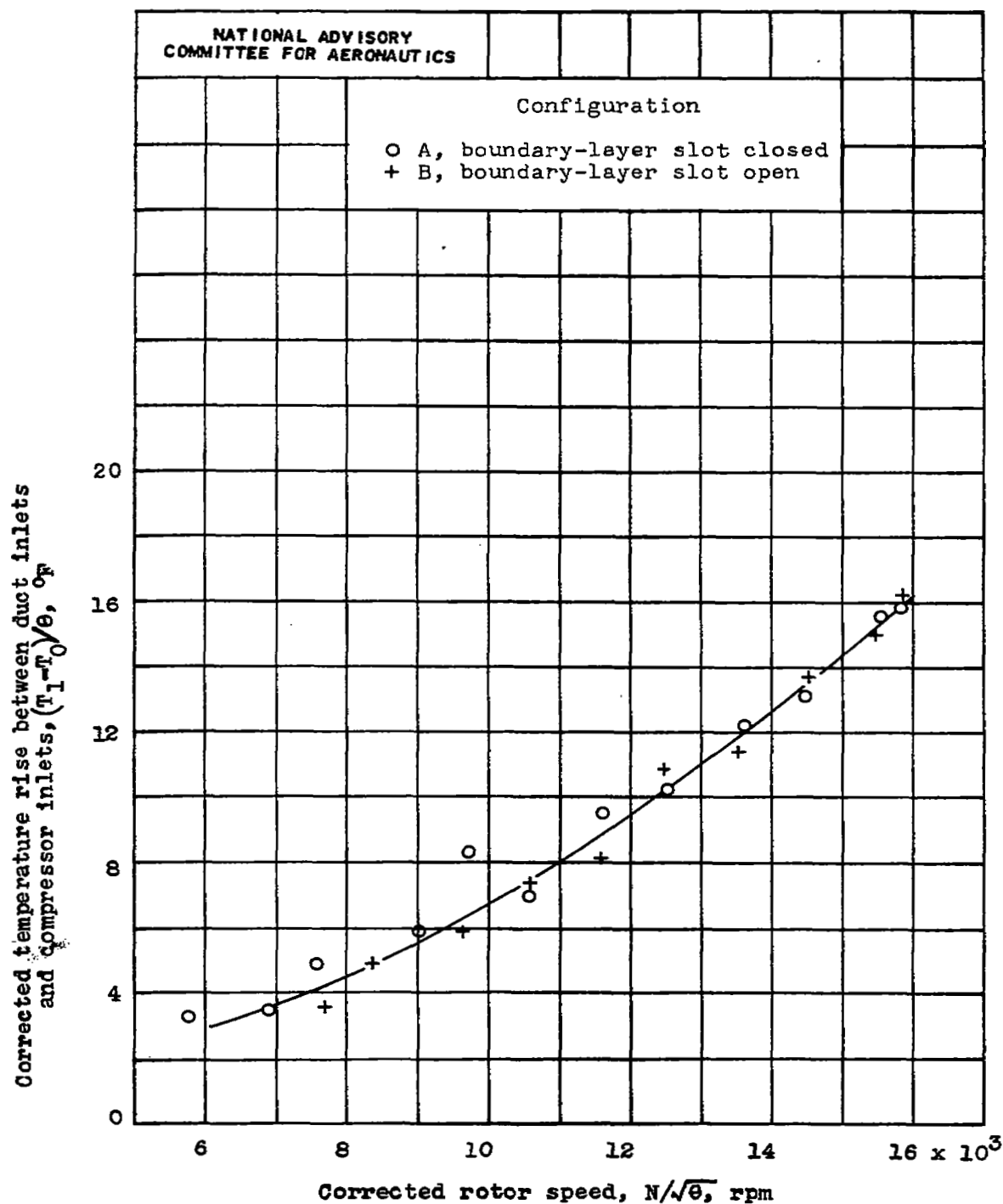
Figure 7. – Temperature rise across XFR-1 duct for configurations A and B used to estimate comparative inlet temperatures for configurations without duct (E and F).
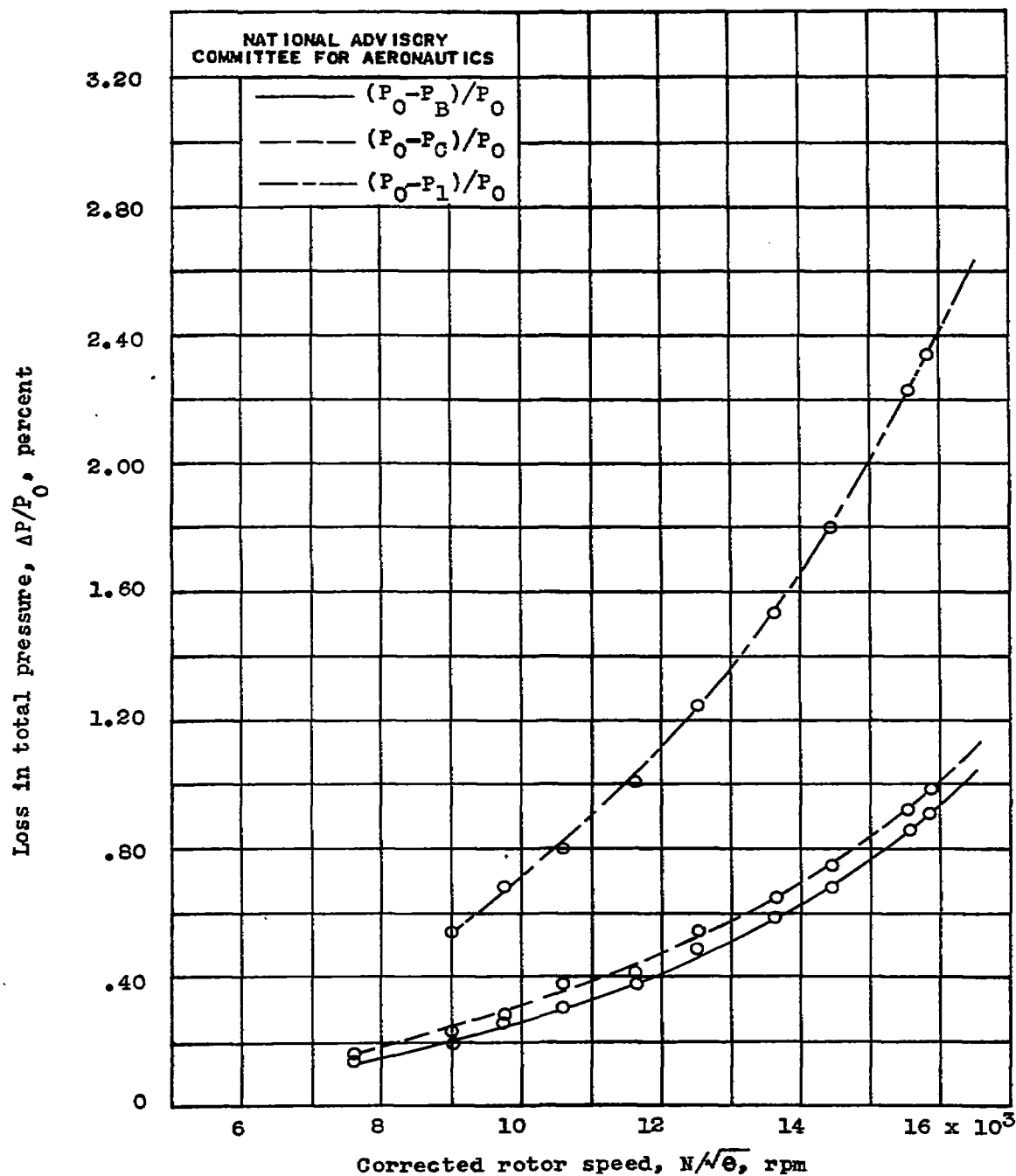
(a) Configuration A, boundary-layer slot closed; XFR-1 tail pipe.

Figure 8. – Loss in total pressure between inlets of XFR-1 intake duct
and various stations of intake duct.
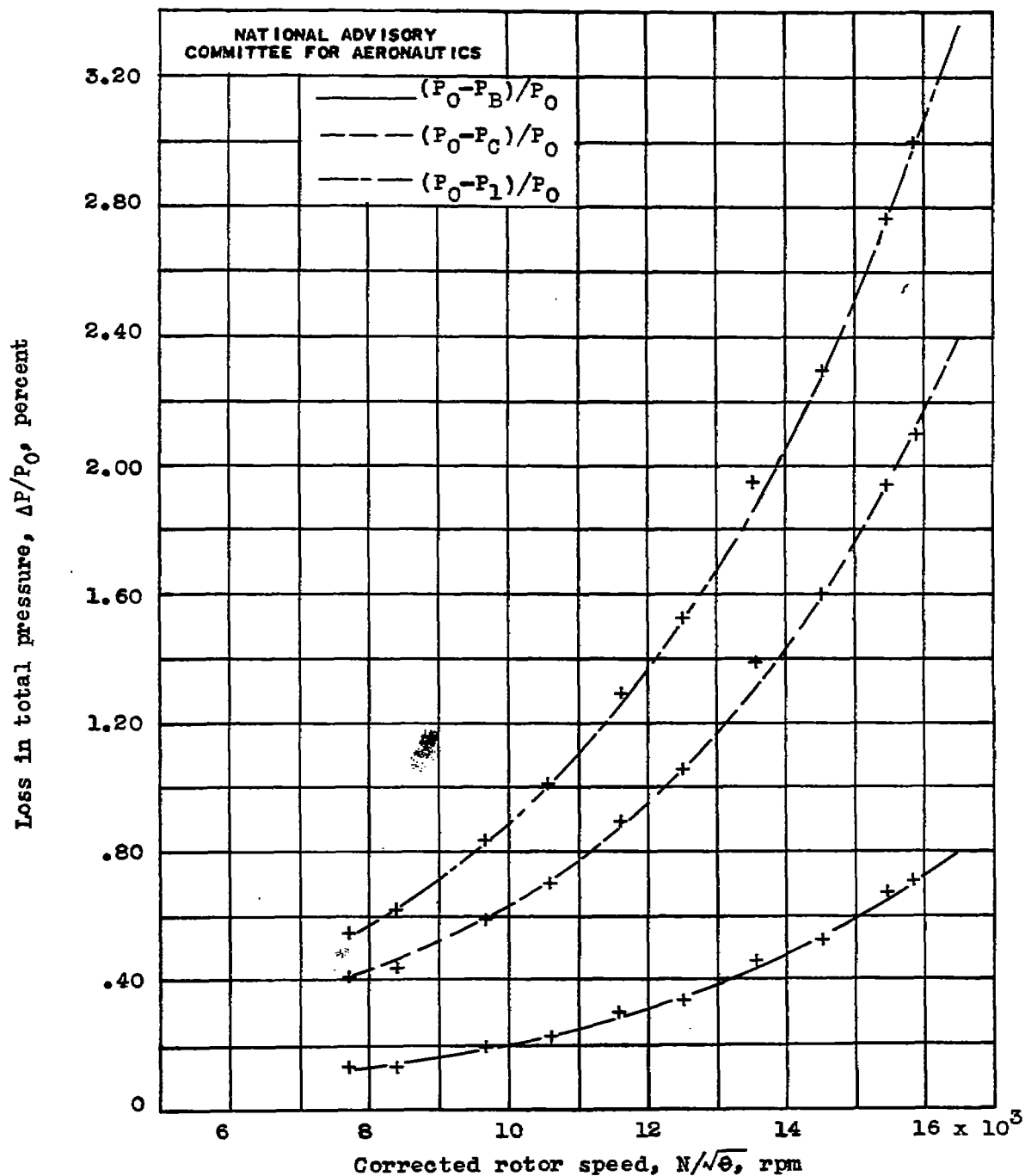
(b) Configuration B, boundary-layer slot open; XFR-1 tail pipe.
Figure 8. — Continued. Loss in total pressure between inlets of XFR-1
intake duct and various stations of intake duct.

(c) Configuration C, boundary-layer removal; XFR-1 tail pipe.

Figure 8. - Continued. Loss in total pressure between inlets of XFR-1
intake duct and various stations of intake duct.

NATIONAL ADVISORY
COMMITTEE FOR AERONAUTICS

Legend:
- $(P_0 - P_B)/P_0$
- $(P_0 - P_C)/P_0$
- $(P_0 - P_1)/P_0$

Y-axis: Loss in total pressure, $\Delta P/P_0$, percent

X-axis: Corrected rotor speed, $N/\sqrt{\theta}$, rpm
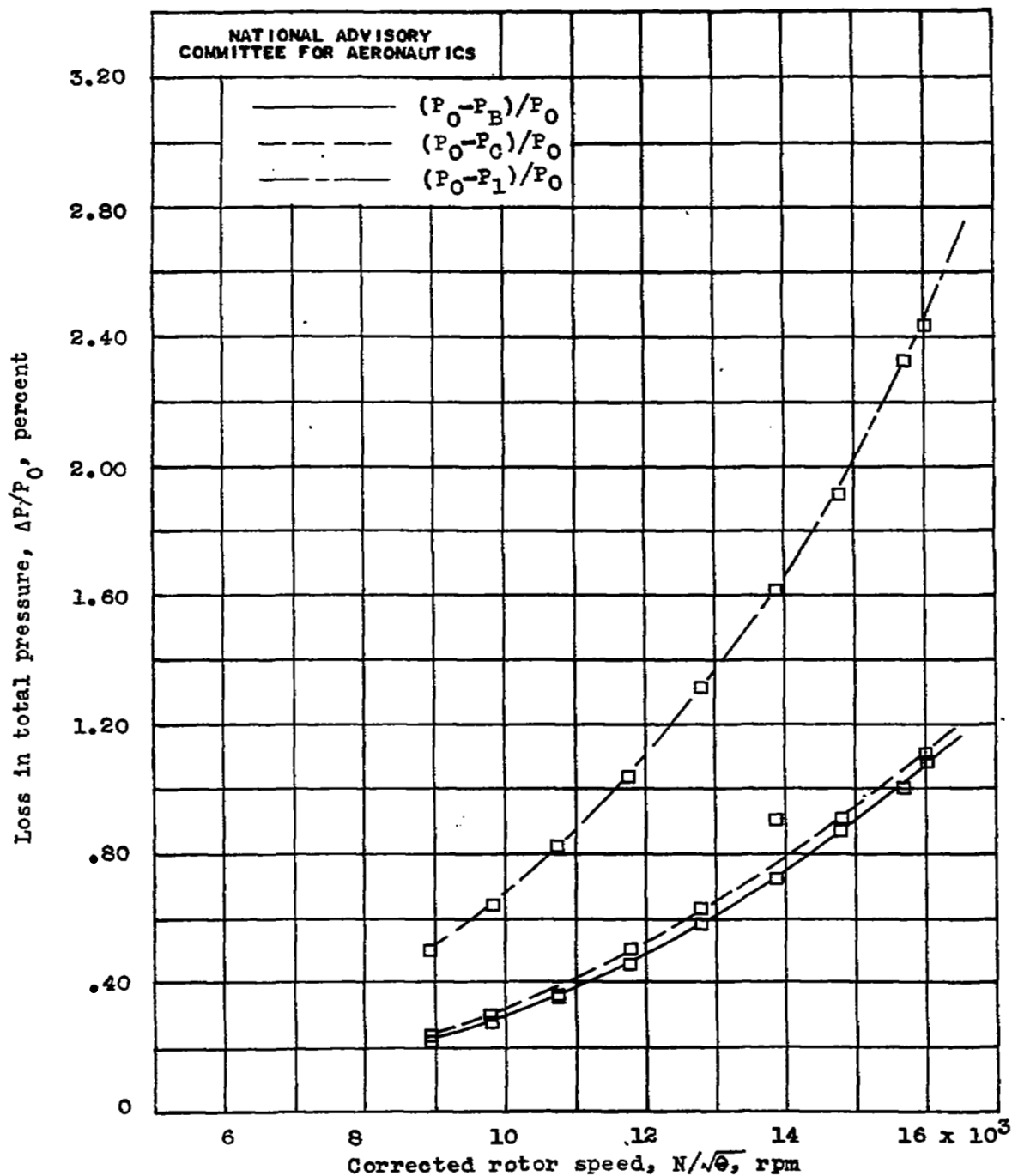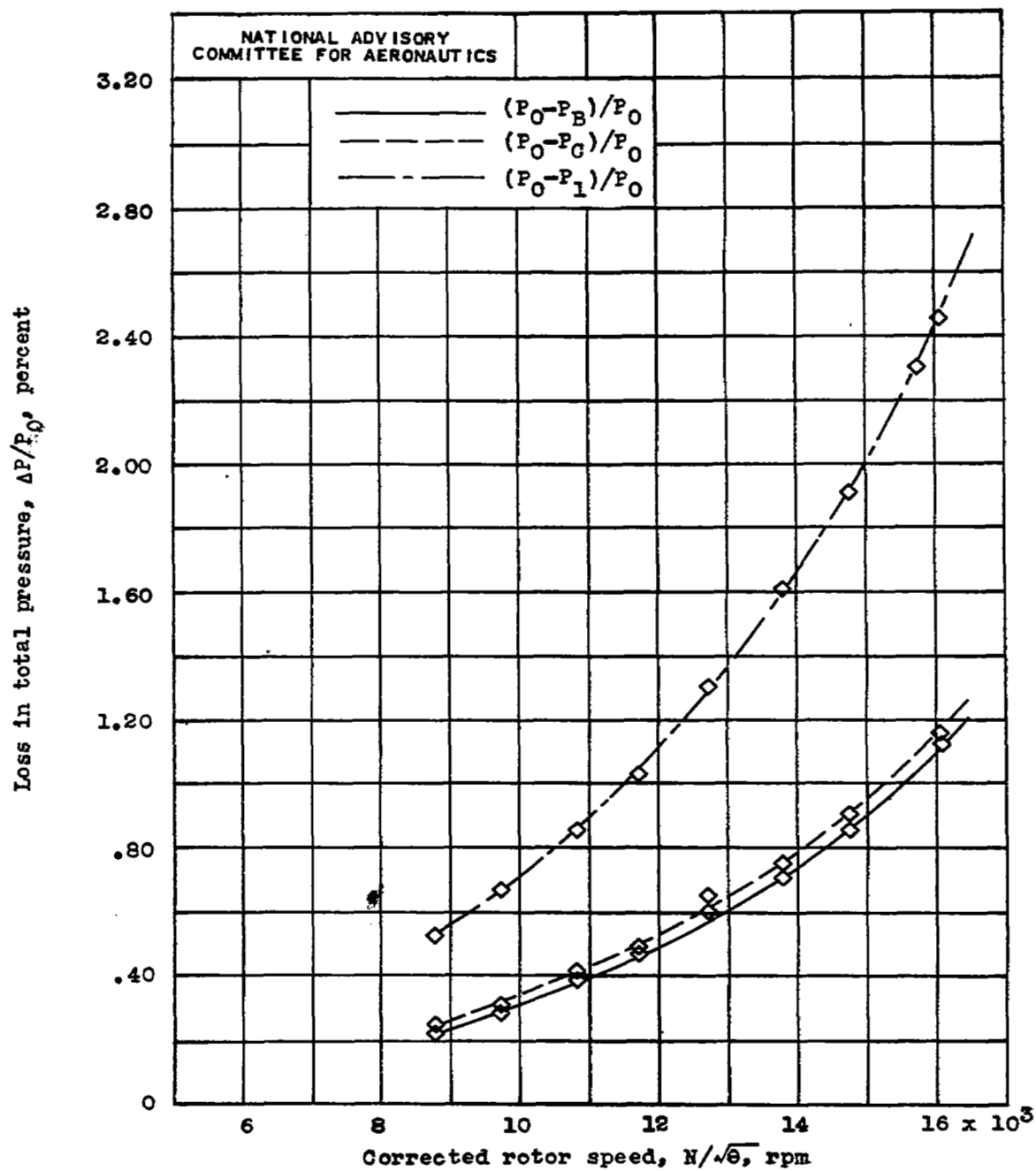
(d) Configuration D, boundary-layer removal; P-59A tail pipe.

Figure 8. - Concluded. Loss in total pressure between inlets of XFR-1 intake duct and various stations of intake duct.
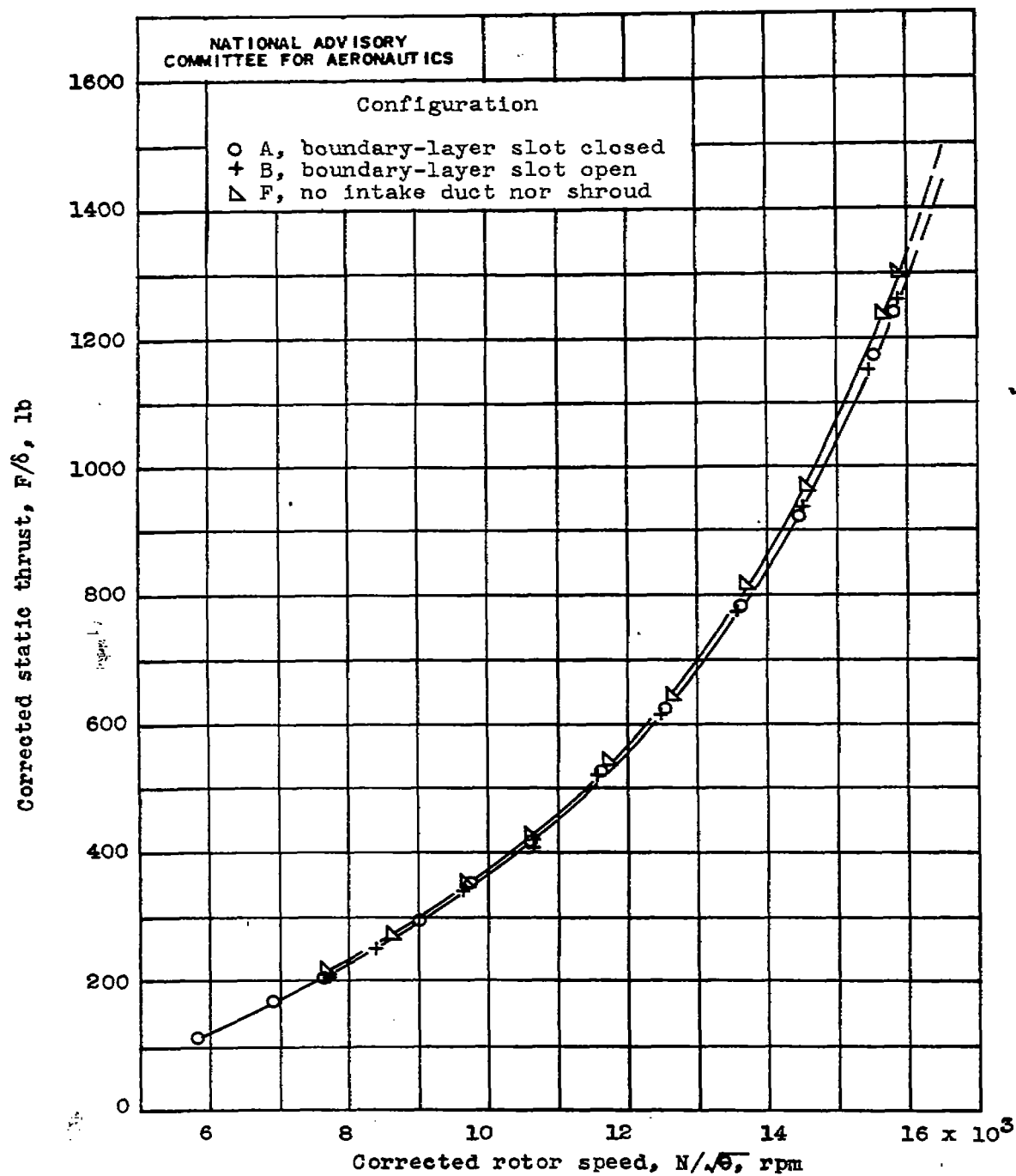
(a) Thrust.

Figure 9. - Comparison of I-16 turbojet engine performance with XFR-1 intake duct in two positions and without intake duct and shroud. XFR-1 tail pipe and nozzle.
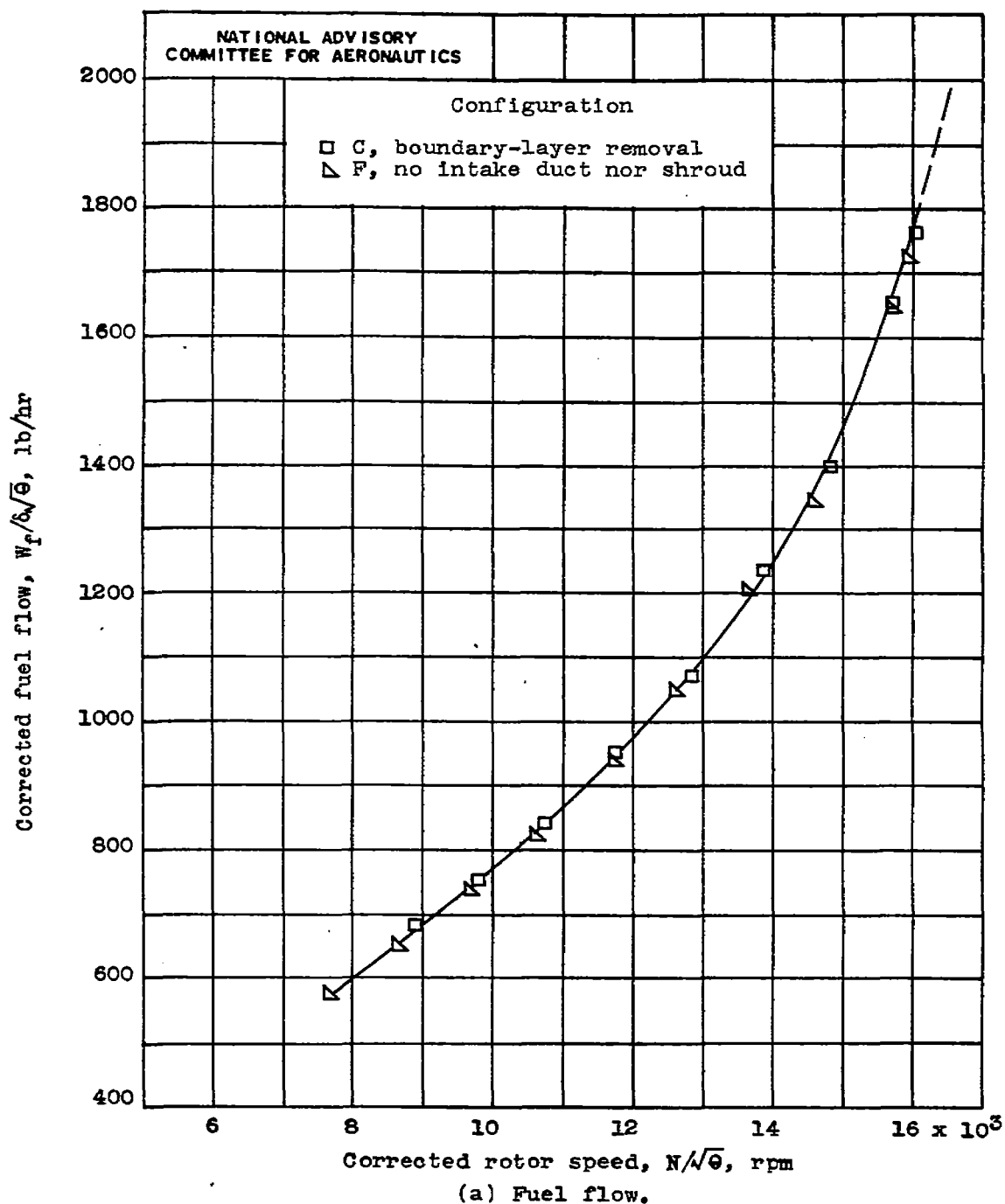
Figure 9. – Continued. Comparison of I-16 turbojet engine performance
with XFR-I intake duct in two positions and without intake duct and
shroud. XFR-I tail pipe and nozzle.

Figure 9. - Continued. Comparison of I-16 turbojet engine performance with XFR-I intake duct in two positions and without intake duct and shroud. XFR-I tail pipe and nozzle.

**NATIONAL ADVISORY
COMMITTEE FOR AERONAUTICS**

Configuration

O A, boundary-layer slot closed
+ B, boundary-layer slot open
△ F, no intake duct nor shroud
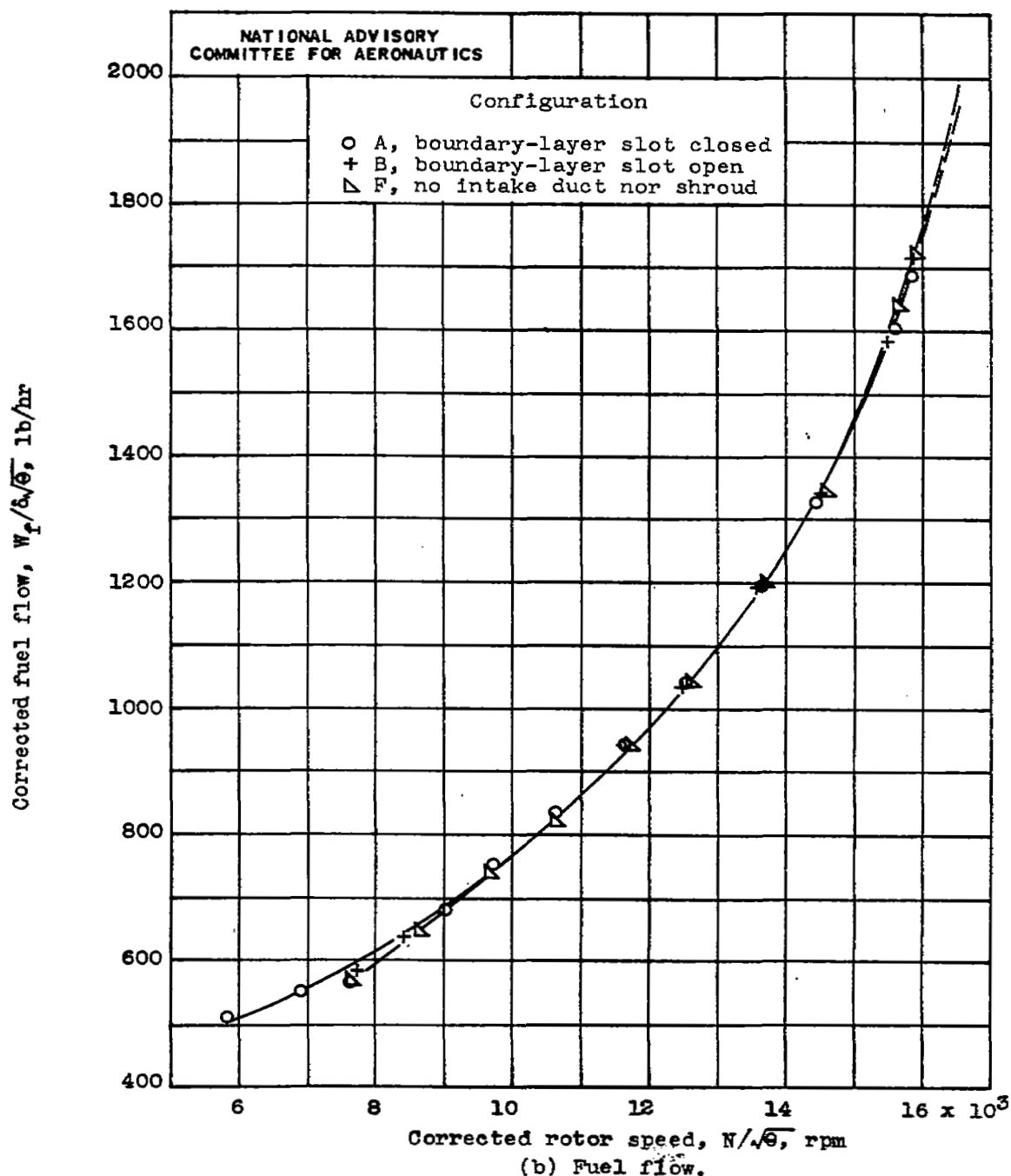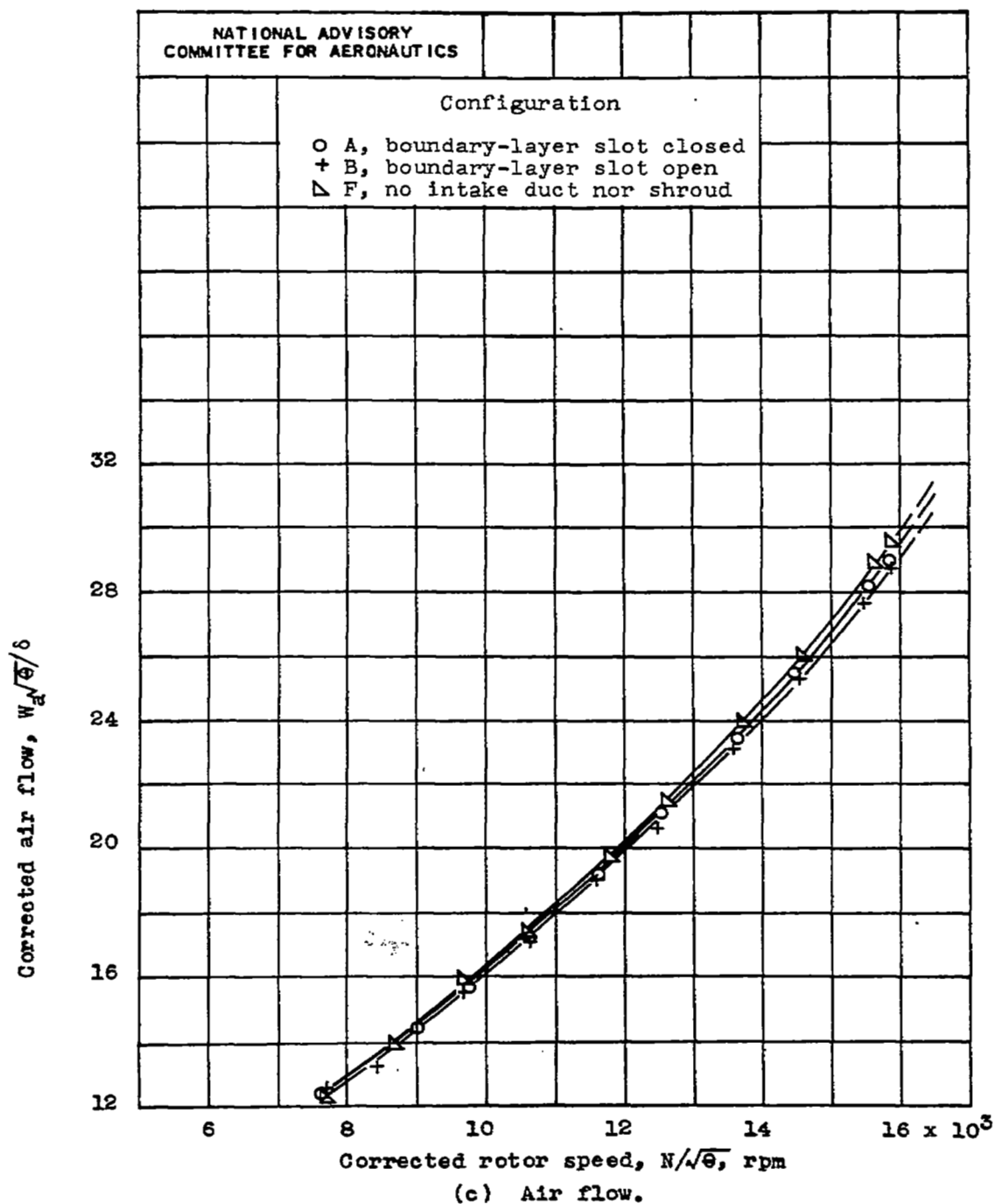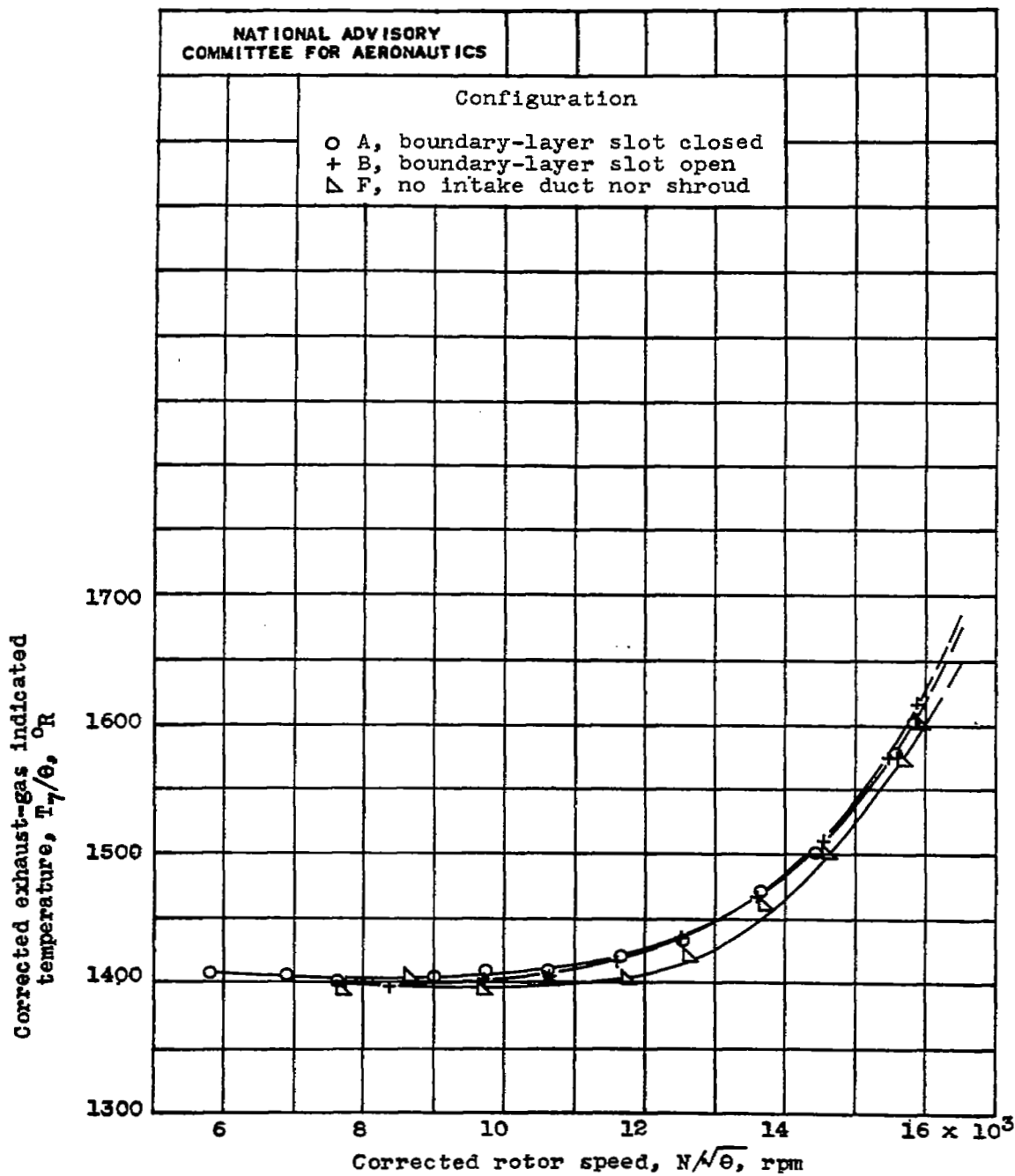
(d) Exhaust-gas indicated temperature.

Figure 9. - Concluded. Comparison of I-16 turbojet engine performance
with XFR-1 intake duct in two positions and without intake duct and
shroud. XFR-1 tail pipe and nozzle.

(a) Fuel flow.

Figure 10. – Comparison of I-16 turbojet engine performance with removal
of boundary layer from XFR-1 intake duct and with intake duct and
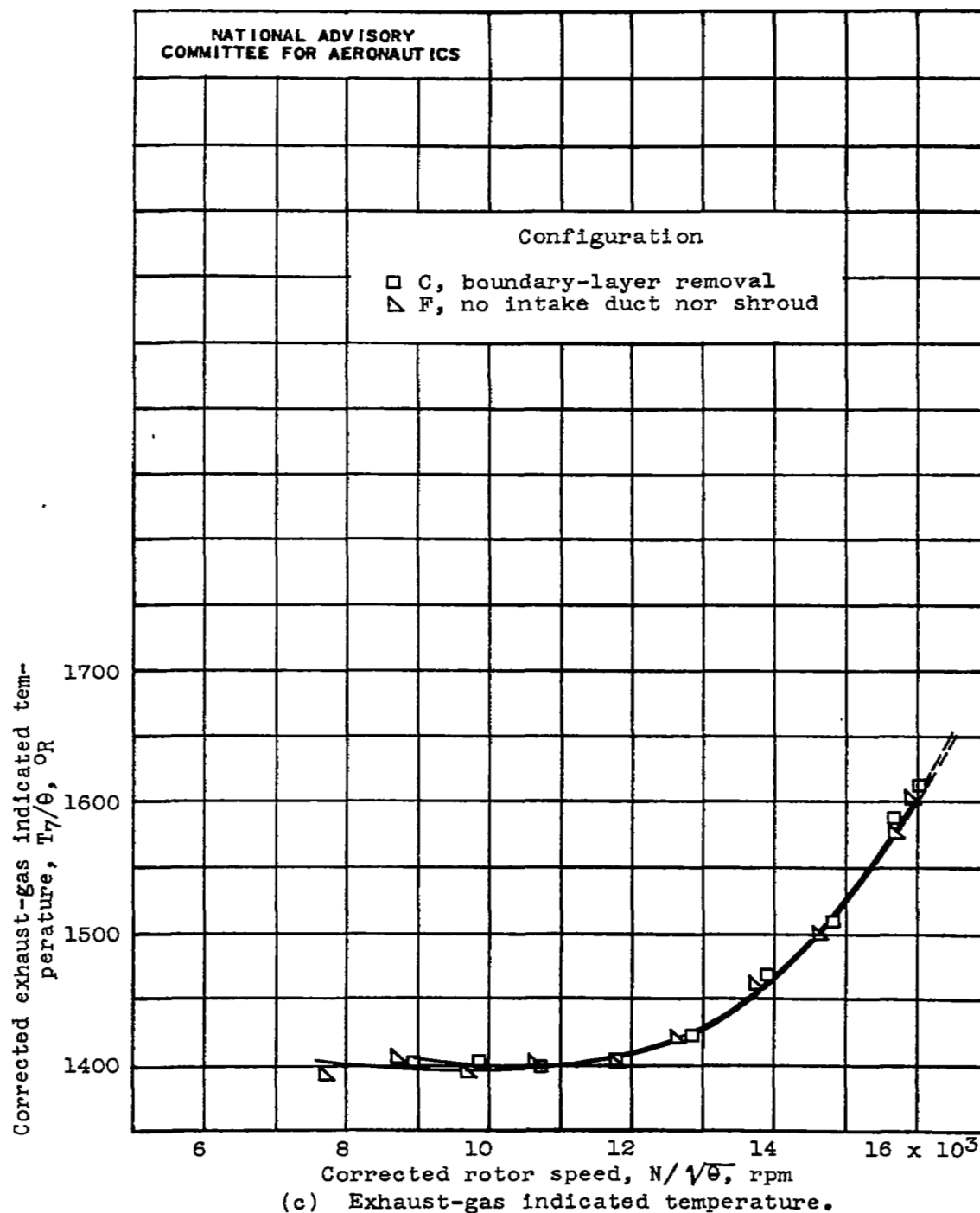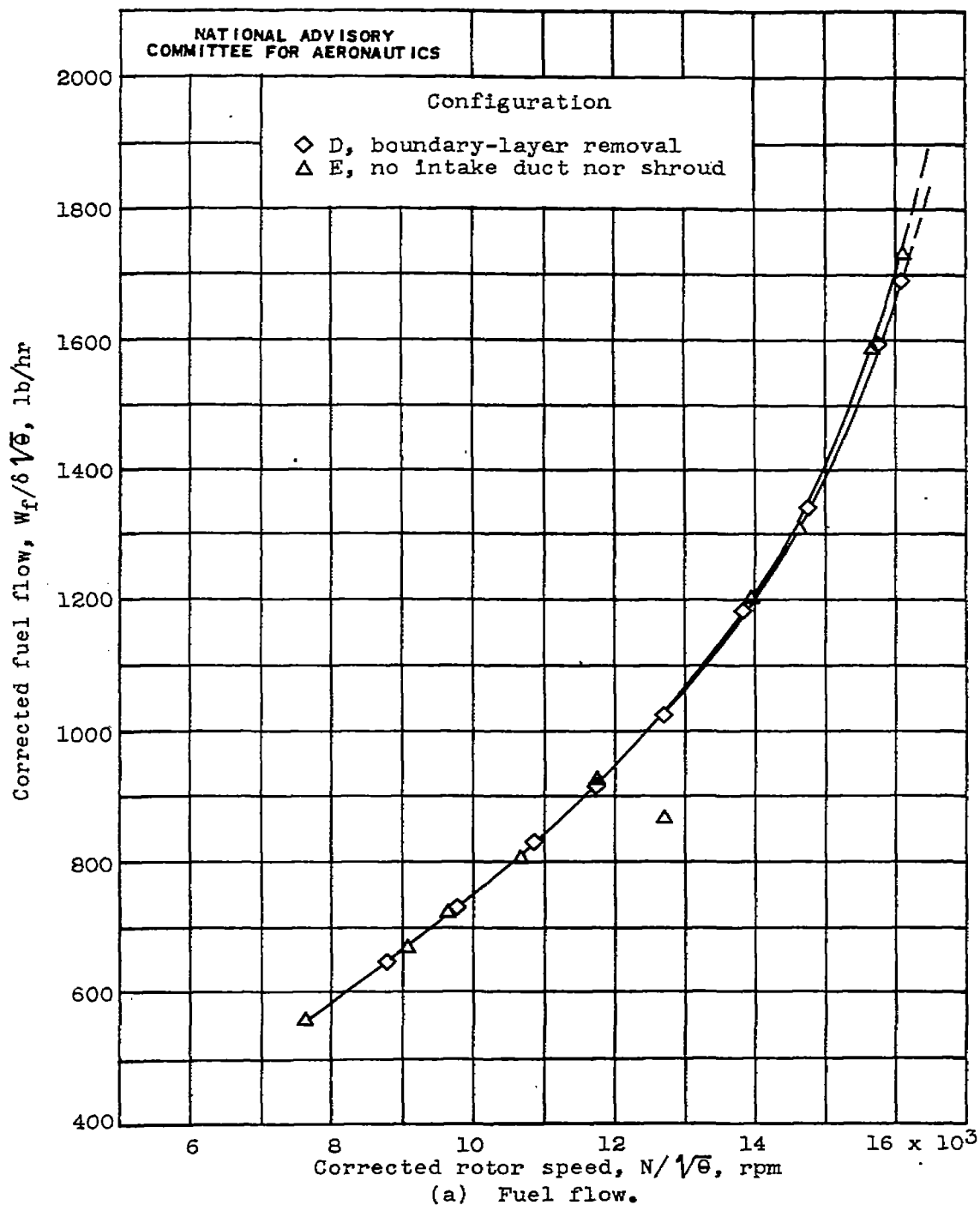shroud removed. XFR-1 tail pipe and nozzle.

(b) Air flow.
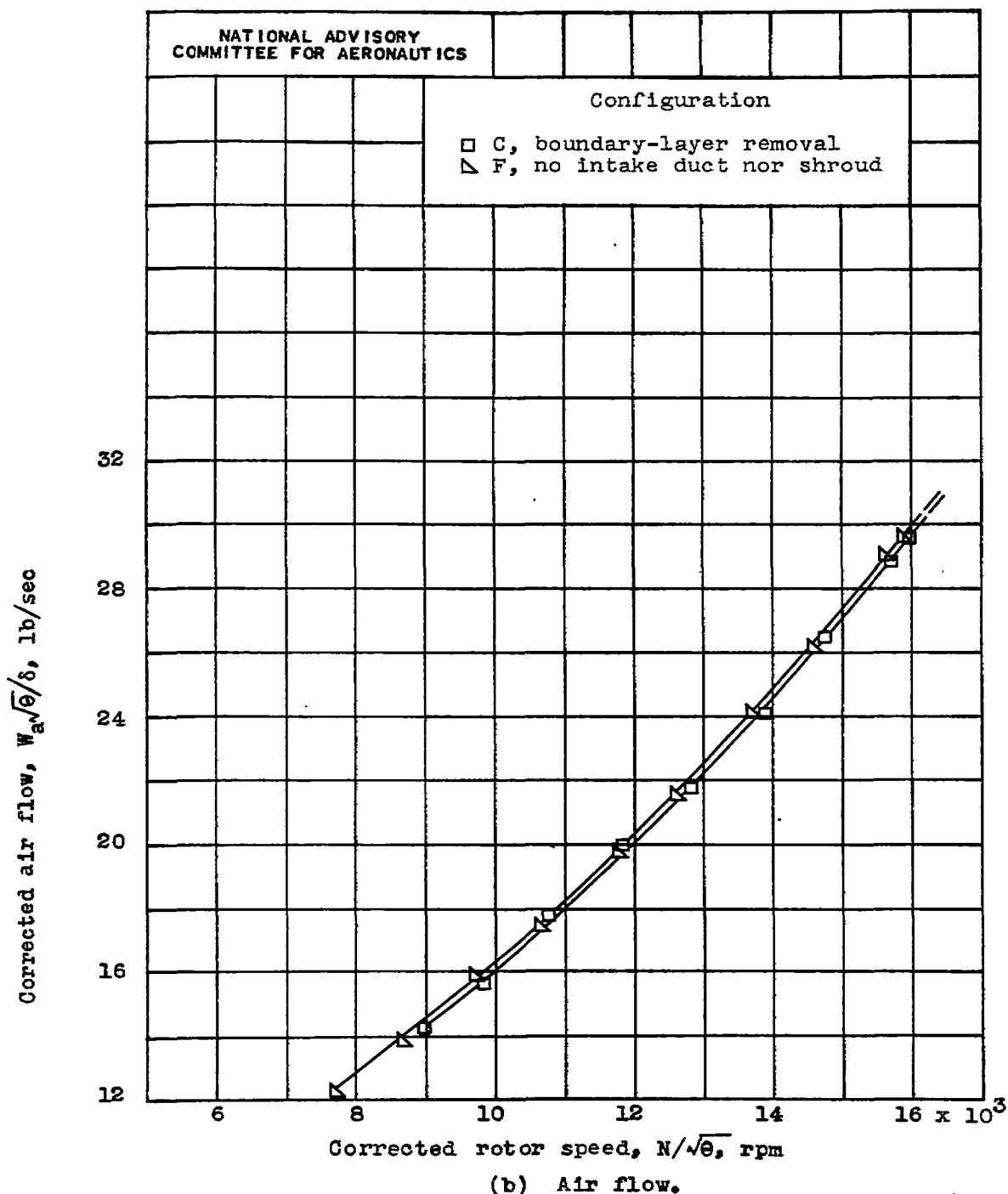
Figure 10. - Continued. Comparison of I-16 turbojet engine performance
with removal of boundary layer from XFR-1 intake duct and with intake
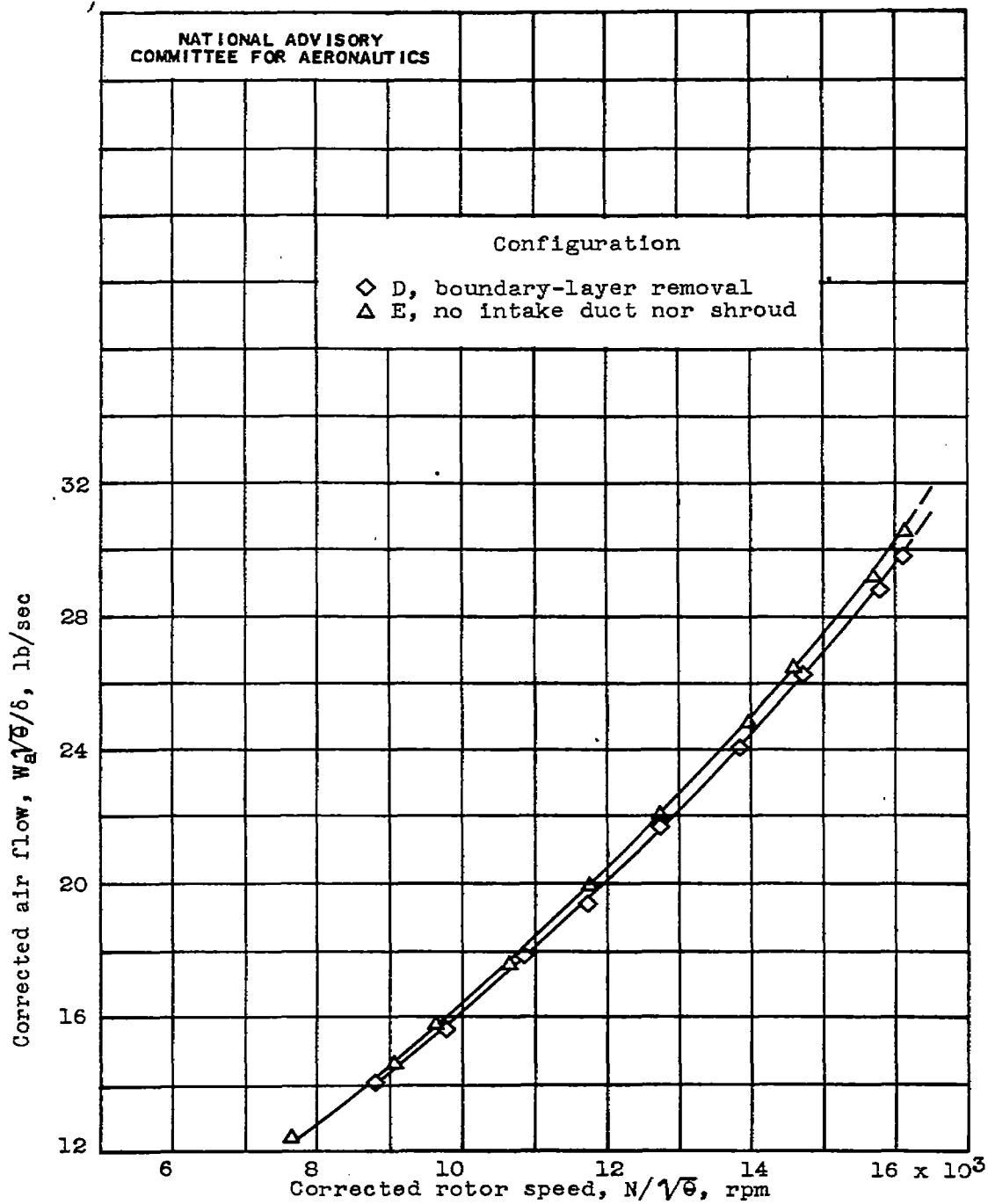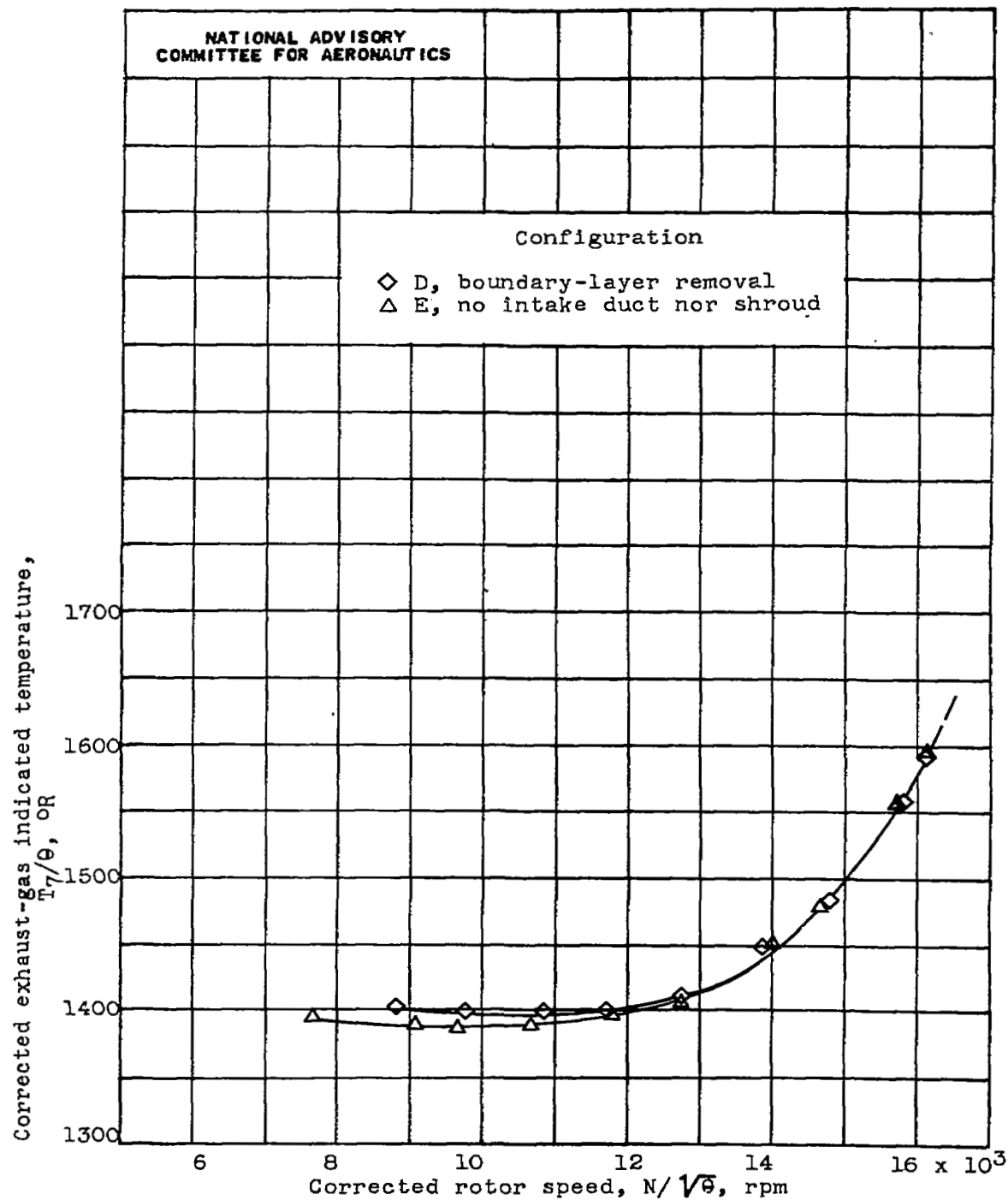duct and shroud removed. XFR-1 tail pipe and nozzle.

Configuration

□ C, boundary-layer removal
△ F, no intake duct nor shroud

(c) Exhaust-gas indicated temperature.

Figure 10. – Concluded. Comparison of I-16 turbojet engine performance
with removal of boundary layer from XFR-1 intake duct and with intake
duct and shroud removed. XFR-1 tail pipe and nozzle.

Figure 11. – Comparison of I-16 turbojet engine performance with removal of boundary layer from XFR-1 intake duct and with intake duct and shroud removed. P-59A tail pipe and nozzle.

NATIONAL ADVISORY
COMMITTEE FOR AERONAUTICS

Configuration

◇ D, boundary-layer removal
△ E, no intake duct nor shroud

(b) Air flow.

Figure 11. - Continued. Comparison of I-16 turbojet engine performance
with removal of boundary layer from XFR-1 intake duct and with intake
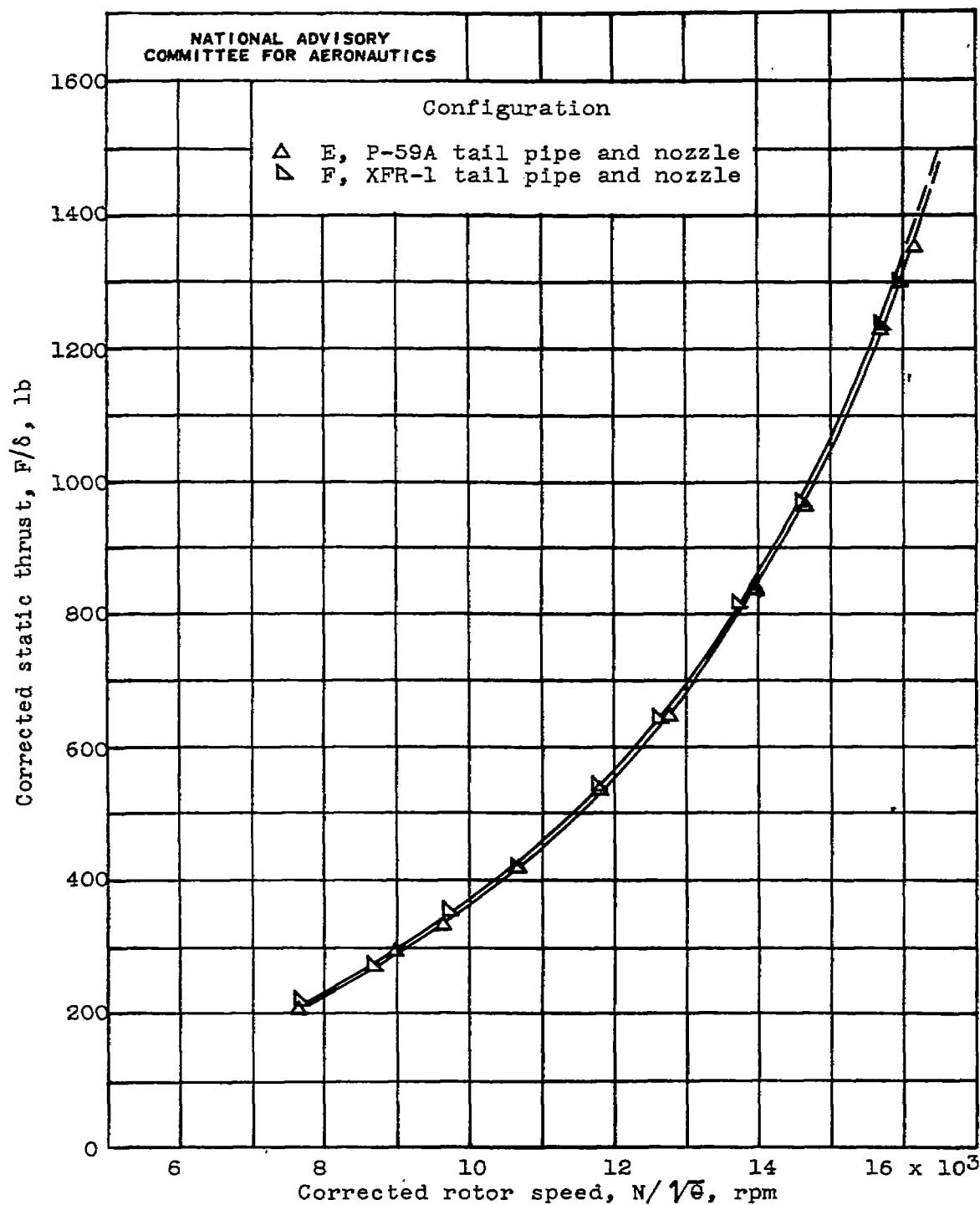duct and shroud removed. P-59A tail pipe and nozzle.

NATIONAL ADVISORY
COMMITTEE FOR AERONAUTICS

Configuration

◇ D, boundary-layer removal
△ E, no intake duct nor shroud

(c)   Exhaust-gas indicated temperature.

Figure II. — Concluded. Comparison of I-16 turbojet engine performance
   with removal of boundary layer from XFR-I intake duct and with intake
   duct and shroud removed. P-59A tail pipe and nozzle.

Figure 12. - Comparison of thrust of I-16 turbojet engine equipped with P-59A tail pipe and nozzle and with the XFR-1 tail pipe and nozzle. No intake duct nor shroud.
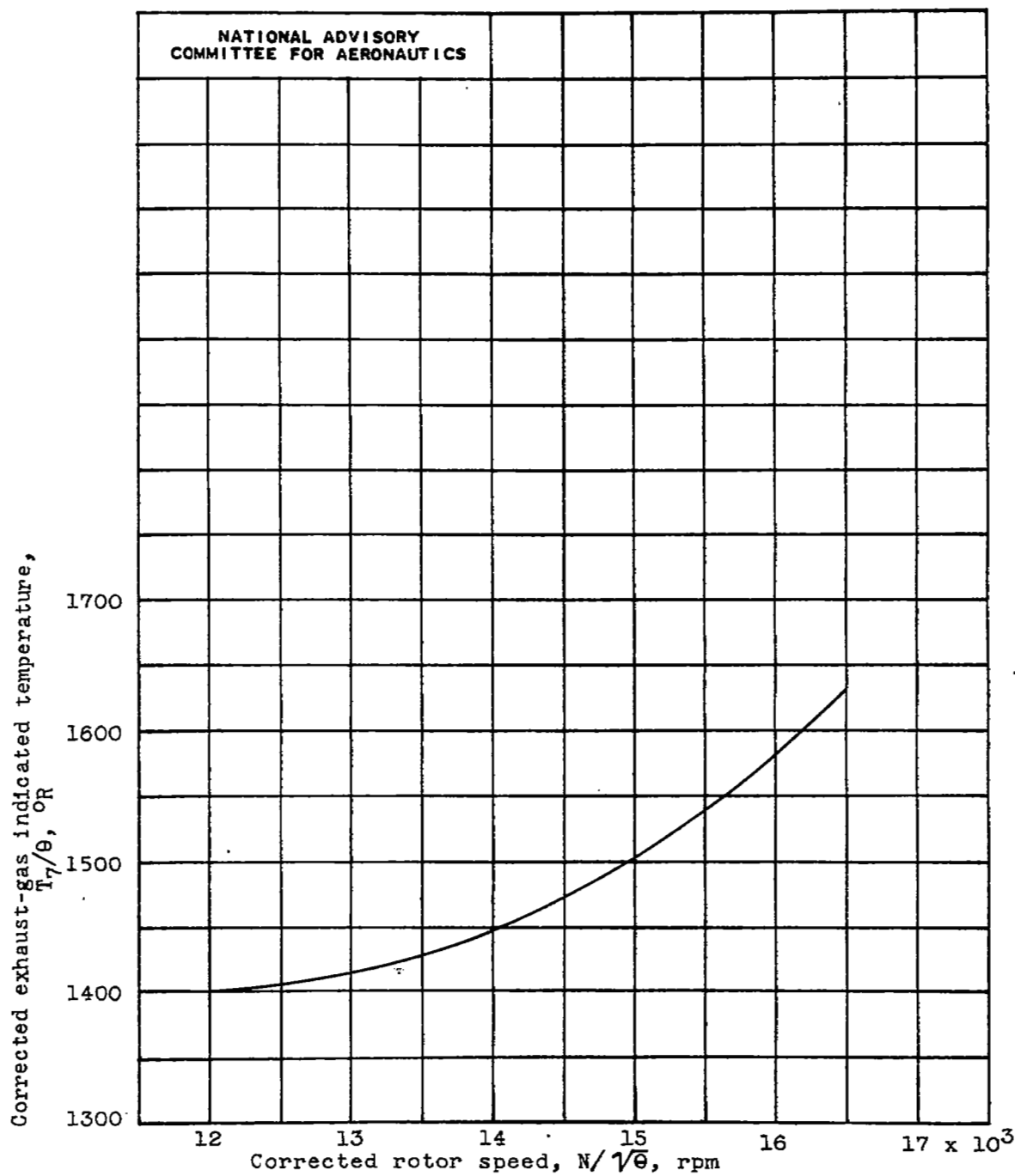
Figure 13. – Exhaust-gas indicated temperature for configuration E to which data from other configurations were adjusted. P–59A tail pipe and nozzle; no intake duct nor shroud. (Replotted from fig. 11(c).)
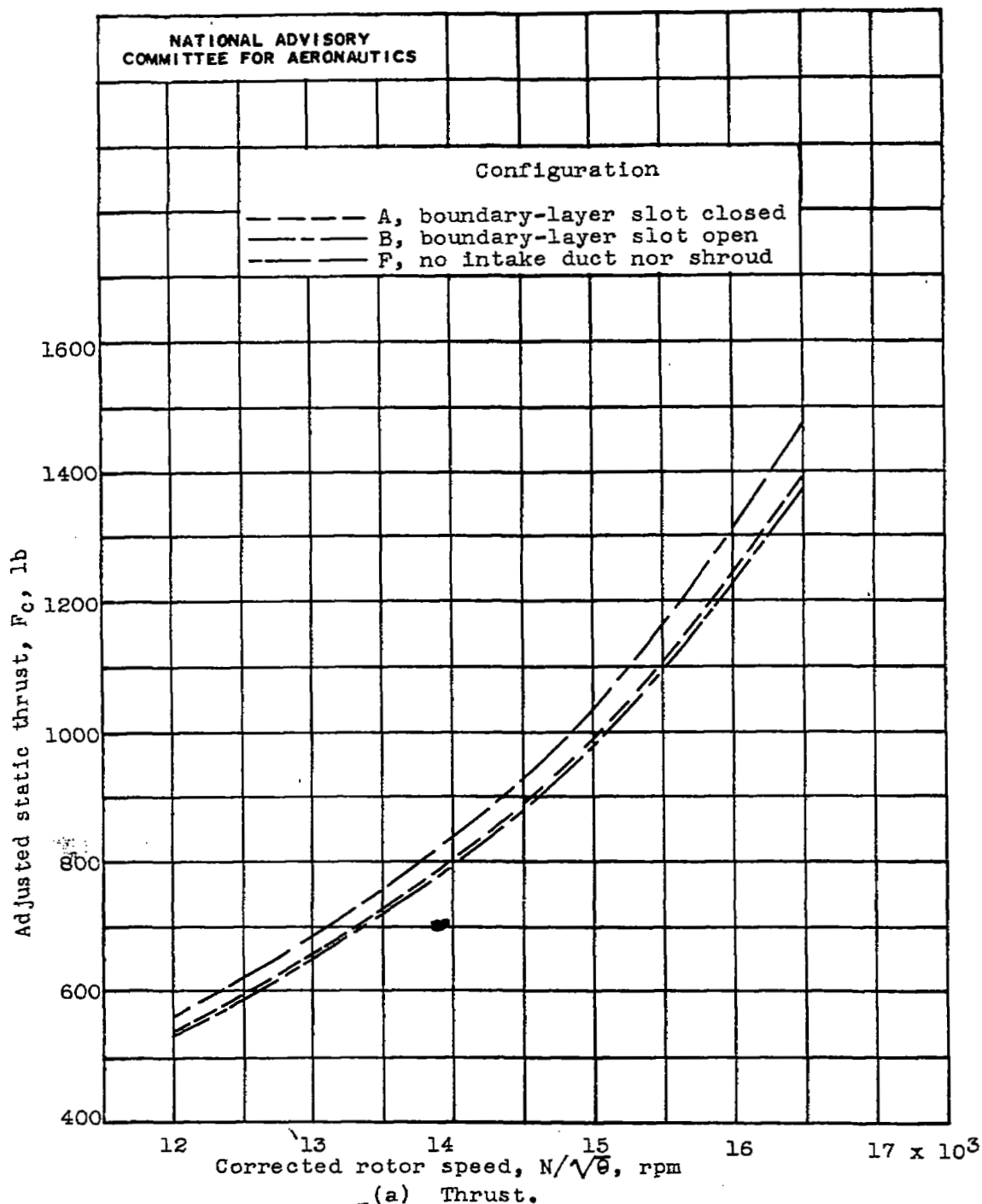
(a)　Thrust.

Figure 14. – Comparison of adjusted I-16 turbojet engine performance
with XFR-1 intake duct in two positions and with intake duct and
shroud removed.　XFR-1 tail pipe and nozzle.　Data adjusted to ex-
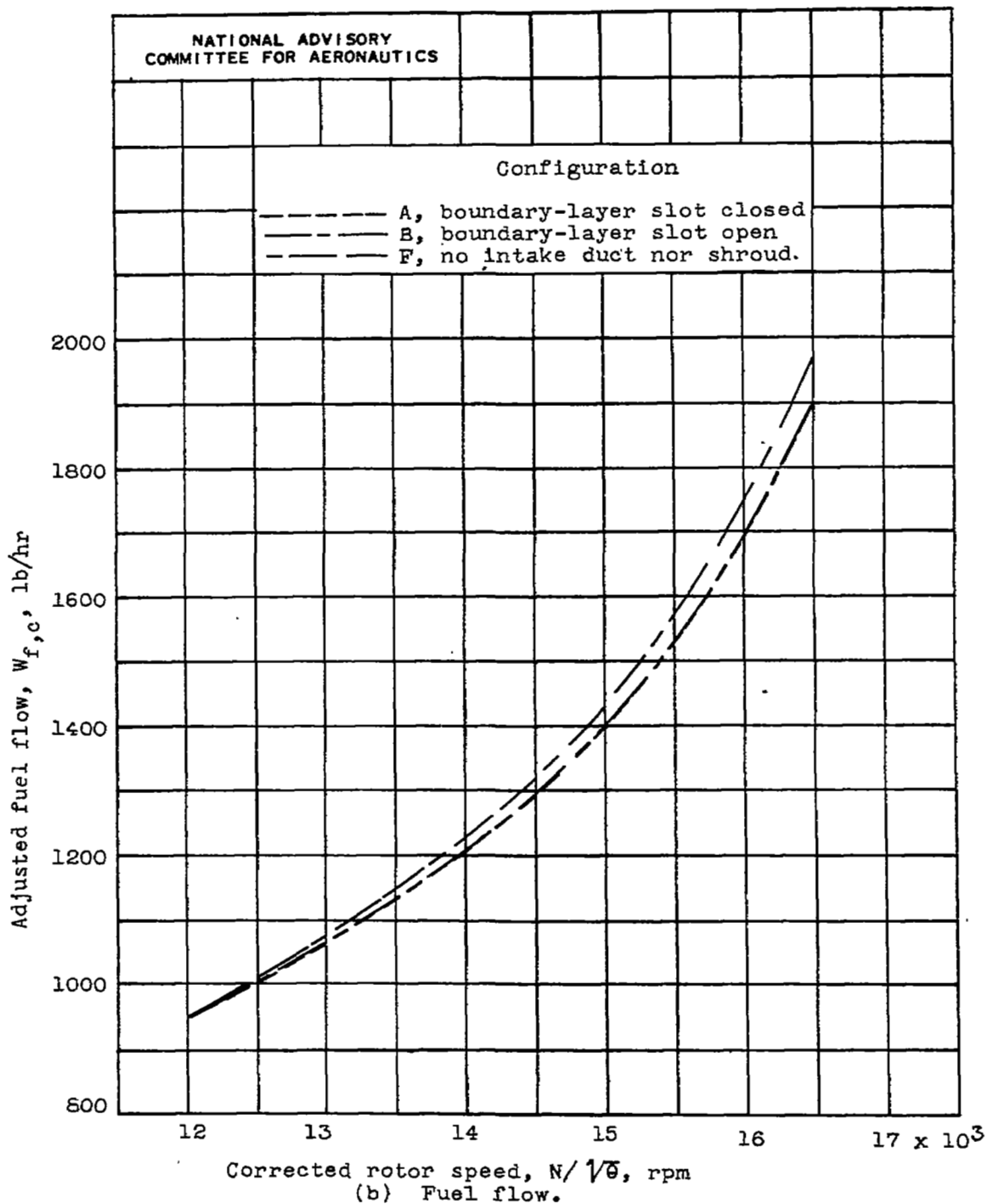haust-gas indicated temperature of configuration E.

Figure 14. - Continued. Comparison of adjusted I-16 turbojet engine performance with XFR-1 intake duct in two positions and with intake duct and shroud removed. XFR-1 tail pipe and nozzle. Data adjusted to exhaust-gas indicated temperature of configuration E.
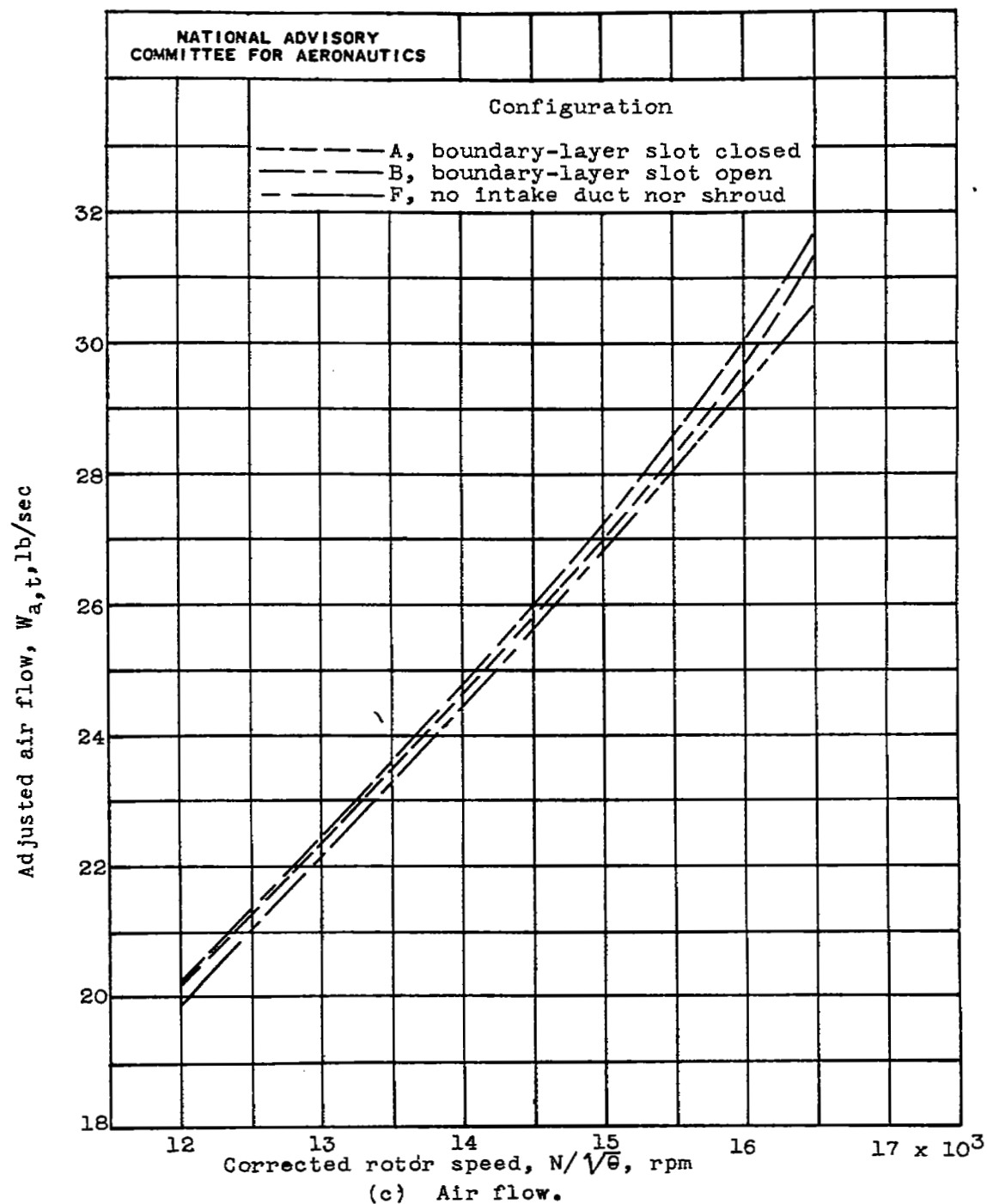
(c) Air flow.

Figure 14. - Continued.　Comparison of adjusted I-16 turbojet engine performance with XFR-I intake duct in two positions and with intake duct and shroud removed.　XFR-I tail pipe and nozzle.　Data adjusted to exhaust-gas indicated temperature of configuration E.

NATIONAL ADVISORY
COMMITTEE FOR AERONAUTICS

Configuration
------------ A, boundary-layer slot closed
----- - ---- B, boundary-layer slot open
--- - --- F, no intake duct nor shroud

Adjusted specific fuel consumption, f_c, lb/hr lb thrust

1.8
1.7
1.6
1.5
1.4
1.3

12   13   14   15   16   17 x 10^3

Corrected rotor speed, $N/\sqrt{\theta}$, rpm
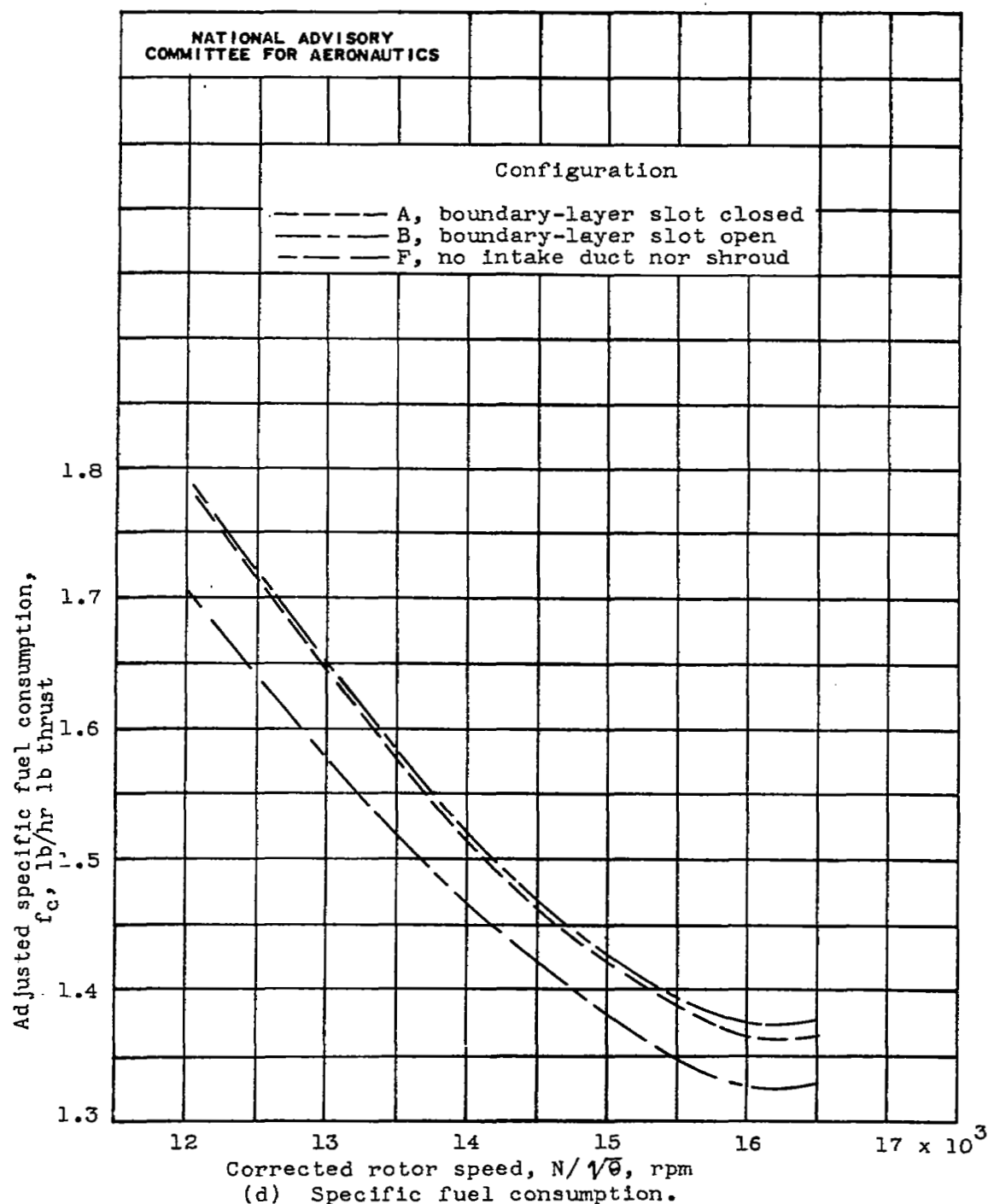
(d)   Specific fuel consumption.

Figure 14. - Concluded.   Comparison of adjusted I-16 turbojet engine
performance with XFR-1 intake duct in two positions and with intake
duct and shroud removed.   XFR-1 tail pipe and nozzle.   Data adjusted
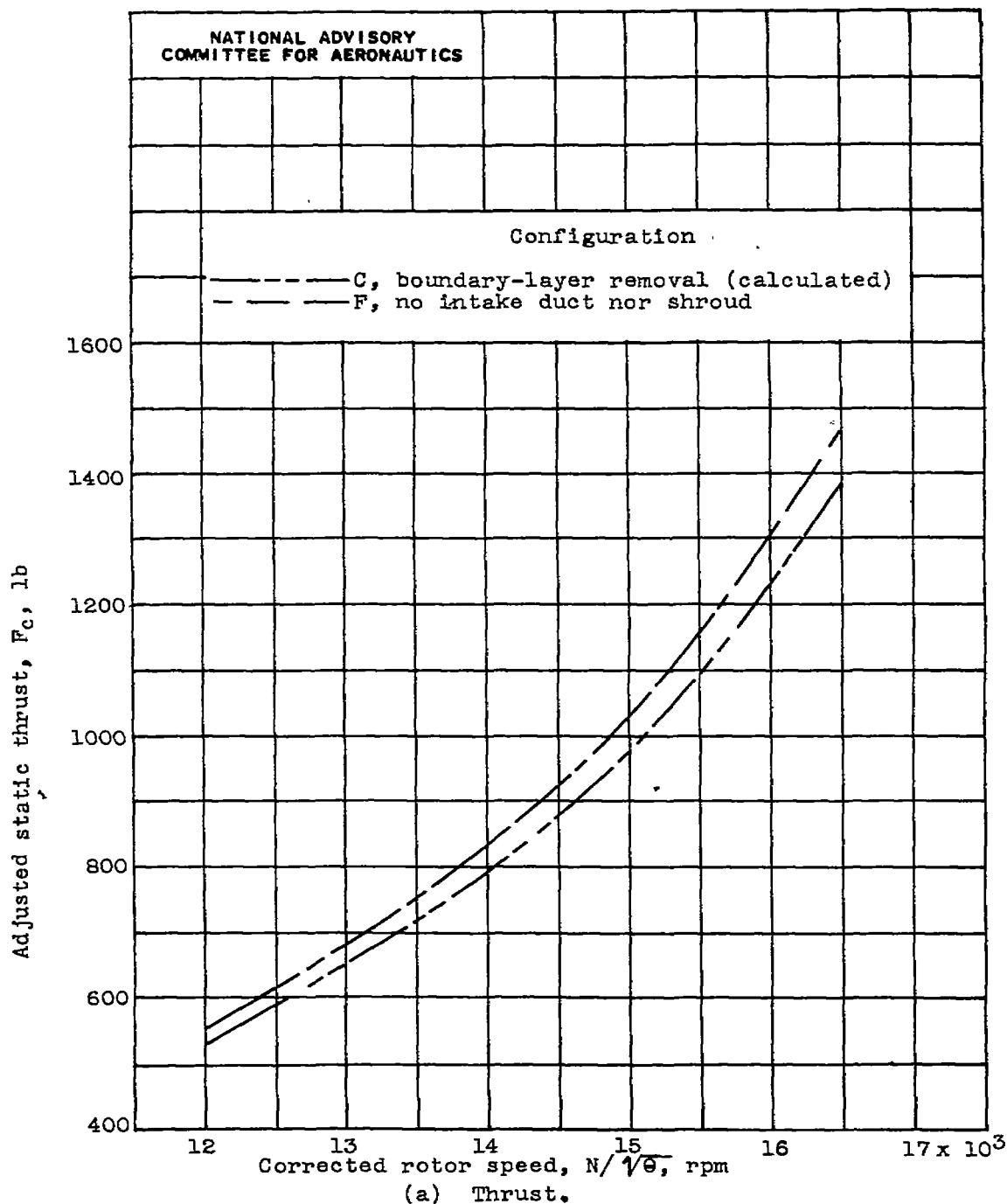to exhaust-gas indicated temperature of configuration E.

Figure 15. - Comparison of adjusted I-16 turbojet engine performance
with removal of boundary layer from XFR-1 intake duct and with intake
duct and shroud removed. XFR-1 tail pipe and nozzle. Data adjusted
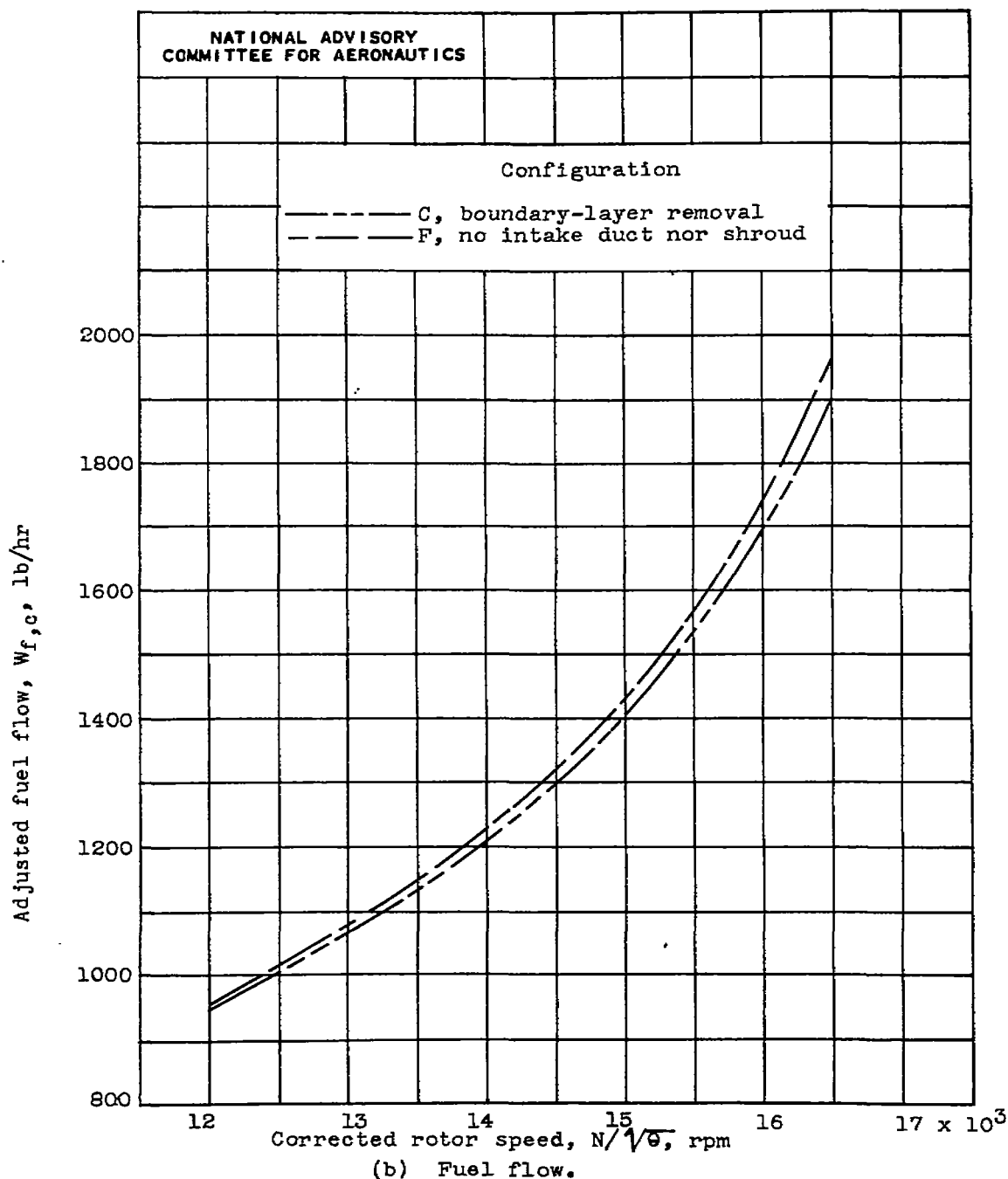to exhaust-gas indicated temperature of configuration E.

Configuration
———————— C, boundary-layer removal
— — — — — F, no intake duct nor shroud

(b)   Fuel flow.

Figure 15. – Continued. Comparison of adjusted I-16 turbojet engine
   performance with removal of boundary layer from XFR-I intake duct and
   with intake duct and shroud removed.   XFR-I tail pipe and nozzle.
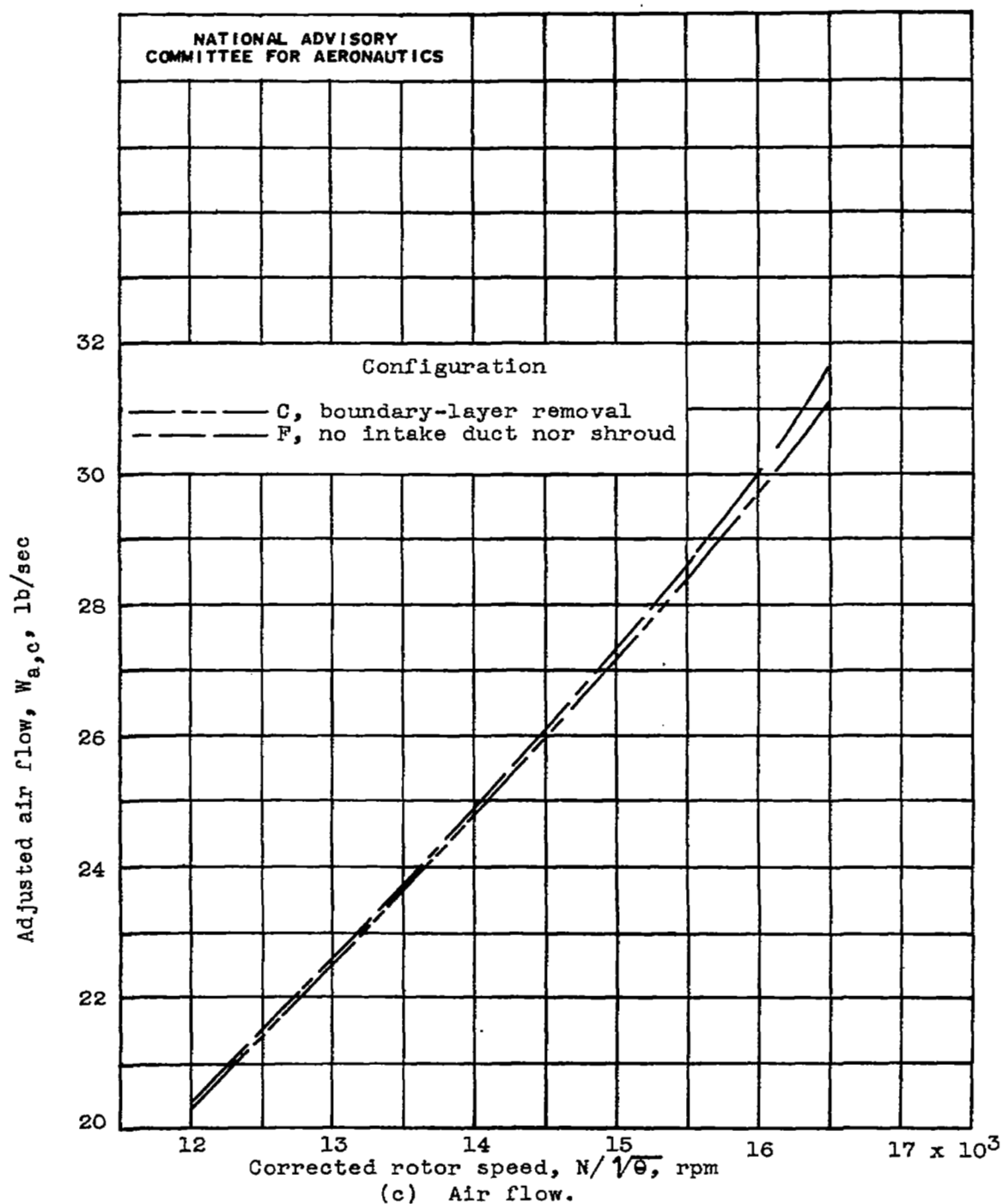   Data adjusted to exhaust-gas indicated temperature of configuration E.

NATIONAL ADVISORY
COMMITTEE FOR AERONAUTICS

Configuration

— — — — — — C, boundary-layer removal
— — — — — F, no intake duct nor shroud

Adjusted air flow, $W_{a,c}$, lb/sec

Corrected rotor speed, $N/\sqrt{\theta}$, rpm

(c) Air flow.

Figure 15. - Continued. Comparison of adjusted I-16 turbojet engine
performance with removal of boundary layer from XFR-1 intake duct and
with intake duct and shroud removed. XFR-1 tail pipe and nozzle.
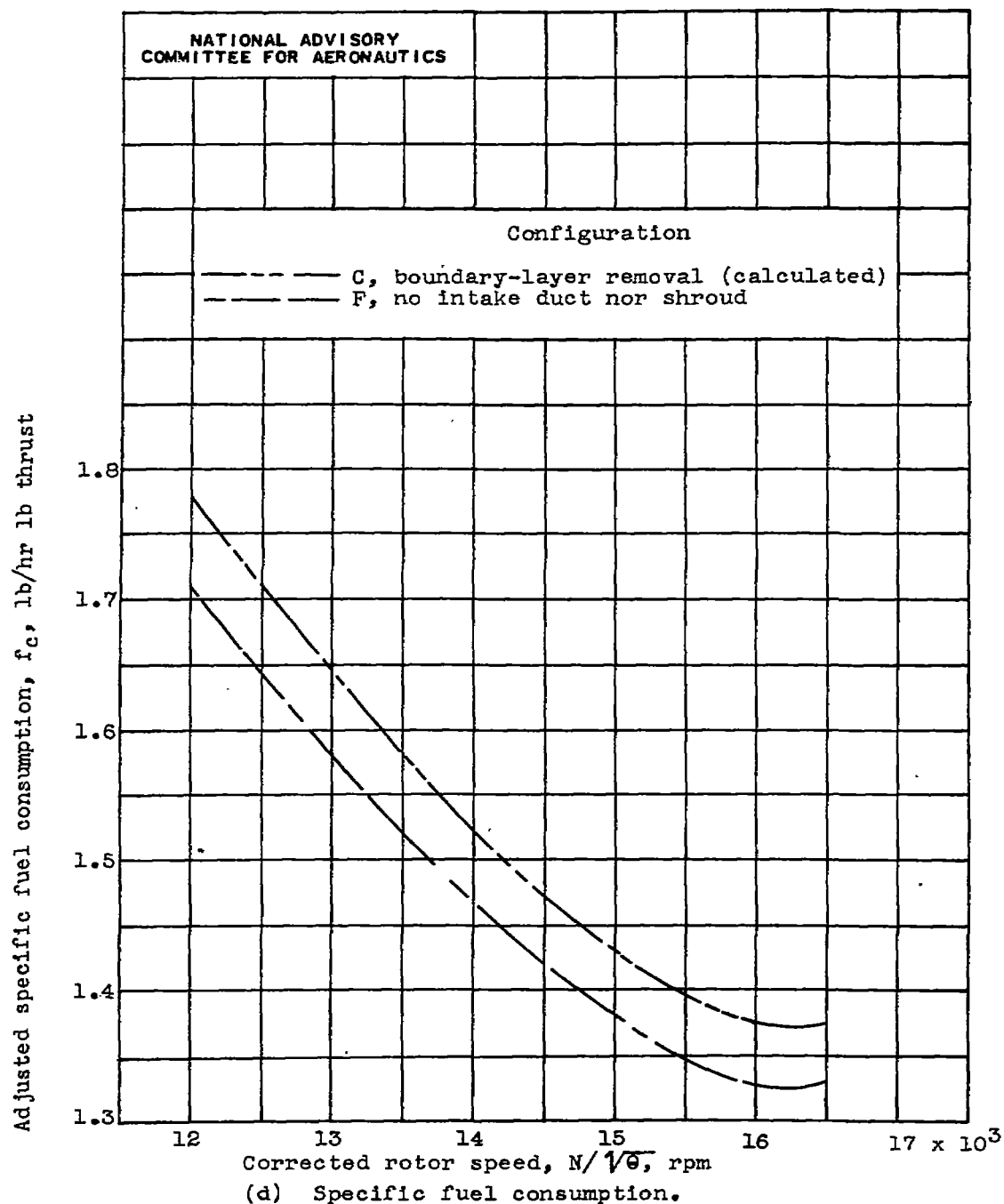Data adjusted to exhaust-gas indicated temperature of configuration E.

(d)   Specific fuel consumption.

Figure 15. – Concluded.   Comparison of adjusted I-16 turbojet engine
performance with removal of boundary layer from XFR-I intake duct and
with intake duct and shroud removed.   XFR-I tail pipe and nozzle.
Data adjusted to exhaust-gas indicated temperature of configuration E.

Configuration

————— ——— D, boundary-layer removal (calculated)
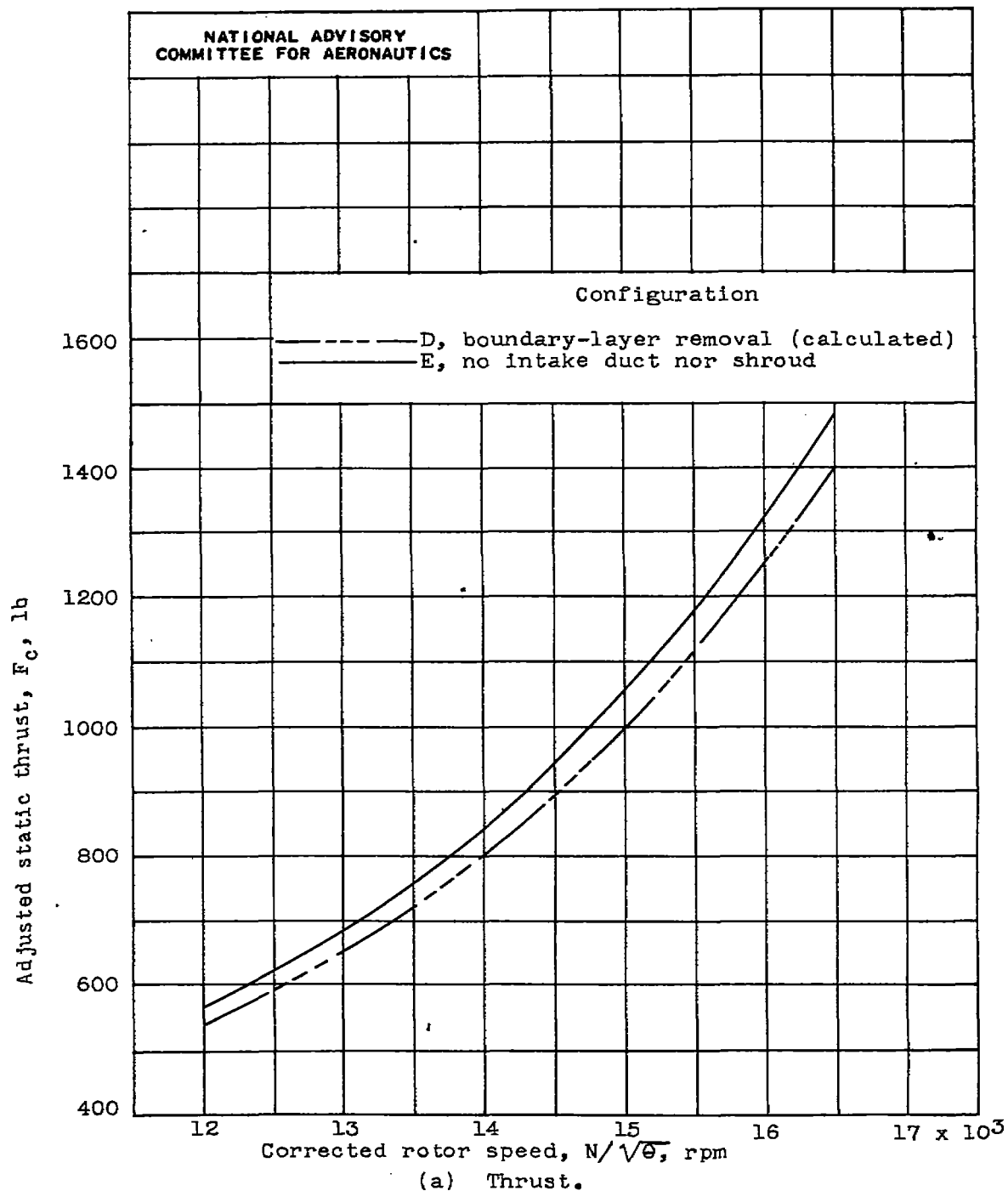——————————E, no intake duct nor shroud

(a)   Thrust.

Figure 16. – Comparison of adjusted I-16 turbojet engine performance
with removal of boundary layer from XFR-1 intake duct and with intake
duct and shroud removed. P-59A tail pipe and nozzle. Data adjusted
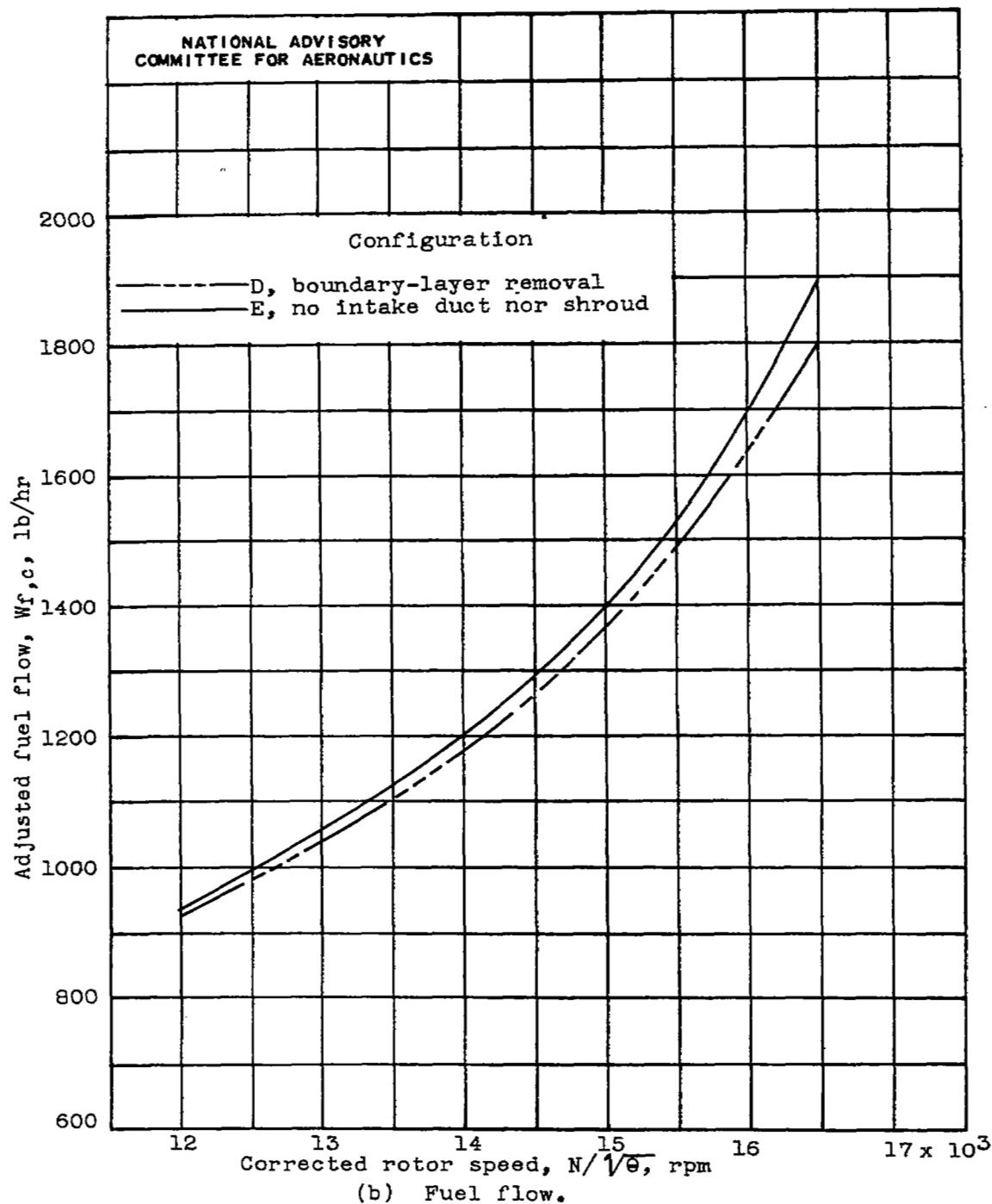to exhaust-gas indicated temperature of configuration E.

NATIONAL ADVISORY
COMMITTEE FOR AERONAUTICS

Configuration

-------- D, boundary-layer removal
———— E, no intake duct nor shroud

Adjusted fuel flow, $W_{f,c}$, lb/hr

Corrected rotor speed, $N/\sqrt{\theta}$, rpm

(b) Fuel flow.

Figure 16. - Continued. Comparison of adjusted I-16 turbojet engine
performance with removal of boundary layer from XFR-I intake duct and
with intake duct and shroud removed. P-59A tail pipe and nozzle.
Data adjusted to exhaust-gas indicated temperature of configuration E.
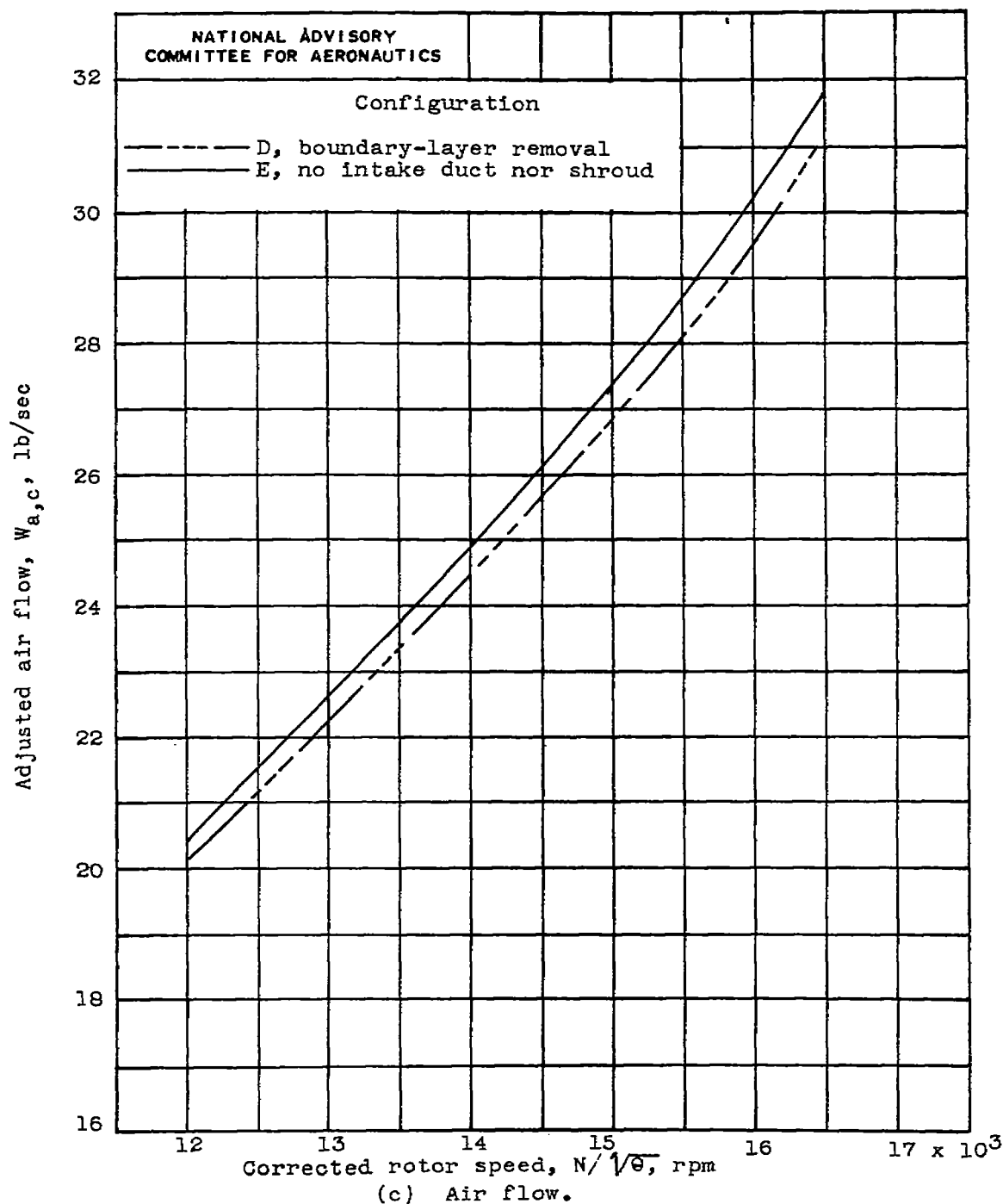
(c) Air flow.

Figure 16. – Continued. Comparison of adjusted I-16 turbojet engine
  performance with removal of boundary layer from XFR-1 intake duct and
  with intake duct and shroud removed. P-59A tail pipe and nozzle.
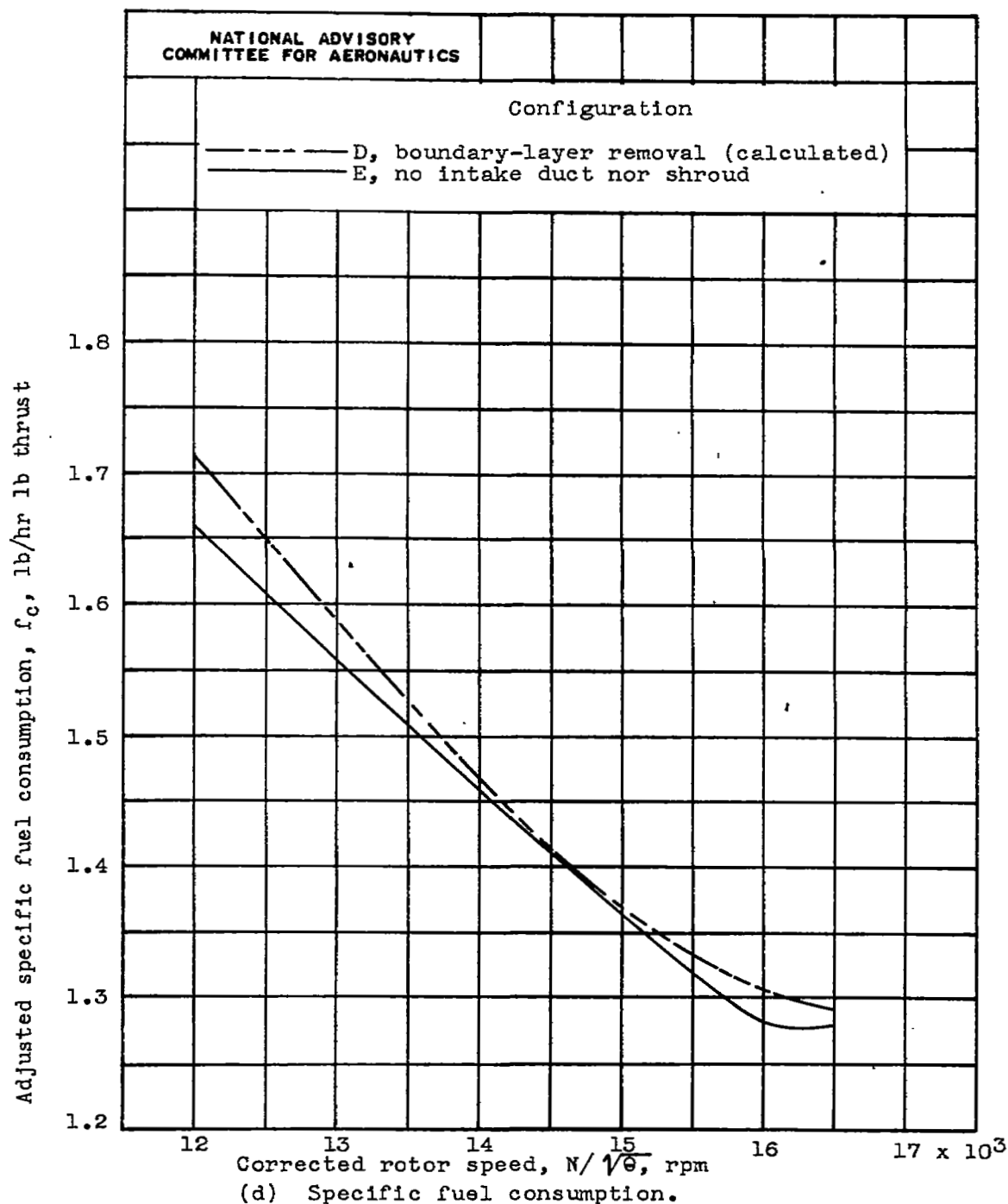 Data adjusted to exhaust-gas indicated temperature of configuration E.

(d) Specific fuel consumption.

Figure 16. – Concluded. Comparison of adjusted I-16 turbojet engine
performance with removal of boundary layer from XFR-1 intake duct and
with intake duct and shroud removed. P-59A tail pipe and nozzle.
Data adjusted to exhaust-gas indicated temperature of configuration E.